Department of Mechanical and Aerospace Engineering

Thermal Storage Modelling and Control for Opportunistic Renewable Charging within a Residential District Heating Scheme at Findhorn Ecovillage

Author: Eli Duggan

Supervisor: Professor Paul Tuohy

A thesis submitted in partial fulfilment for the requirement of degree in

Master of Science in Sustainable Engineering: Renewable Energy Systems and the Environment

August 2024

Copyright Declaration

This thesis is the result of the author's original research. It has been composed by the author and has not been previously submitted for examination which has led to the award of a degree.

Signed: Eli Duggan

Date: Monday August 12th, 2024

Abstract

The threat of anthropogenic global warming necessitates decarbonization across society. In the UK, the residential sector generates a substantial share of emissions that can largely be attributed to space and water heating using fossil fuels. Electrification offers a path away from carbon-intensive heating, provided the electricity is renewably generated. Findhorn Ecovillage has pursued electrification in recent housing developments. The Woodside neighborhood has an electrified district heating network with separate domestic hot water (DHW) and space heating (SH) water tanks charged by a single water-source heat pump (WSHP). Woodside has solar panels and Findhorn has significant wind generation, but supply-demand mismatches still occur frequently. This means surplus renewable electricity is sold cheaply and grid electricity is imported expensively. Shifting water tank charging to better align with renewable generation could enable increased renewables utilisation and decreased cost and carbon intensity.

This thesis exploits the load-shifting potential of Woodside thermal storage using alternative control strategies and novel tariff structures. A first-principles multi-node thermal storage model was adapted from PyLESA to produce separate DHW and SH tank models in Python. Empirical heat loss parameters were introduced and calibrated against monitored data to ensure accurate system representation. These models were then used to simulate the Woodside heating system over a year under three rule-based control (RBC) regimes and five tariffs, including dynamic wind tariffs. Key performance indicators (KPIs) and graphical representations were applied to reveal differences in system behavior across the simulated scenarios.

Simulations demonstrate that advanced RBC can achieve moderate reductions in heating costs for district heating systems with thermal storage. A 12.0% reduction in operational cost of heat (OCOH), from £0.1458/kWh_{th} to £0.1283/kWh_{th}, is calculated using advanced RBC with the second dynamic wind tariff (DWT). This corresponds to an annual cost reduction of ~£250, a 38.4% relative increase in renewables utilisation, and a 21.4% drop in carbon intensity. Graphical analysis shows these reductions are achieved by better aligning charging events with generation and charging to higher node temperatures.

These findings suggest that advanced RBC can synergize with dynamic tariffs to decrease heating costs and carbon intensity while increasing renewables utilisation within community energy schemes. Though not assessed here, predictive controls may offer further benefits. To facilitate future work, the thermal storage models and control scripts developed during this thesis are shared at https://github.com/eli-d-strath/woodside_control.

Acknowledgments

I want to thank my supervisor, Dr Paul Tuohy, for his excellent guidance, feedback, and positivity throughout the project. My thanks extend to PhD student Isaac Whitelaw, who helped massively in learning about the Emoncms portal and accessing Woodside data and fostered a fruitful dialogue about the Woodside heating system. I also thank Dr Graeme Flett for kindly offering answers to multiple questions about his previous versions of the thermal storage models. The previous collaborations between Strathclyde and the Findhorn Foundation have been instrumental in laying the groundwork for this analysis, so I thank everyone involved in those efforts.

I'd like to thank the Fulbright Commission and the University of Strathclyde for funding my MSc through a Fulbright Grant. Finally, I'd like to thank the family and friends who have supported my growth and happiness throughout the MSc and thesis.

Table of Contents

List of Figures

List of Tables

Nomenclature

Symbol	Description
BEMS	Building energy management systems
CFD	Computational fluid dynamics
COP	Coefficient of Performance
CVRMSE	Coefficient of variation for root mean square error
DHW	Domestic hot water
DWT	Dynamic wind tariff
ETP	Energy Technology Partnership
FWP	Findhorn Wind Park
HVAC	Heating, ventilation and air conditioning
KPI	Key performance indicator
MAE	Mean absolute error
MAPE	Mean absolute percentage error
MB	Moving boundary
MPC	Model predictive control
NFD	New Findhorn Directions
OCOH	Operational cost of heat
ORIGIN	Orchestration of Renewable Integrated Generation in Neighborhoods
PET	Park Ecovillage Trust
POCIT	Predictive and Opportunistic Control of Renewable Integrated Thermal Stores
PV	Photovoltaic
RBC	Rule-based control
SH	Space heating
SIES	Smart Integrated Energy Systems
SSEN	Scottish and Southern Energy Networks
SSM	Simple storage model
WSHP	Water source heat pump

1.0 Introduction

This section introduces Findhorn Ecovillage, the Woodside neighborhood, and the energy challenges it faces. The project aims and approach are identified and project scope is discussed.

1.1 Findhorn Ecovillage

Findhorn Ecovillage (hereafter ‘Findhorn’) is a community located along the Moray Firth with homes, offices, shops, and other building types. Findhorn was founded to promote sustainable and ecological lifestyles; in line with this ethos, it has invested significantly in energy efficient housing, sustainable water treatment, and onsite renewable energy. Interesting aspects of their energy system include a privately owned and operated low-voltage distribution network and 675kW of wind capacity in addition to photovoltaic (PV) panels [1]. This private-wire distribution network is connected to the regional Scottish and Southern Energy Networks (SSEN) grid via a 975kW substation. Findhorn undergoes a biannual contract negotiation process through an energy broker with an energy supply company to establish tariff rates for the sale of excess renewables and importation of grid electricity.

Recent developments such as East Whins, West Whins, and Woodside have incorporated heat pumps that facilitate renewable electricity-powered heating. Dwellings have individual heat pumps at East Whins, while dwellings are connected to energy centres with a central heat pump and thermal stores in a district heating scheme at Woodside and West Whins [1]. Residents can choose a standard or day-night tariff scheme. The standard rate is a flat £0.3407/kWh, while the day-night rate charges £0.3607/kWh from 7:00-12:00 and £0.3171/kWh otherwise [2].

Several connected organizations manage the site’s operations. The organizations most relevant to the energy system are New Findhorn Directions (NFD) and Findhorn Wind Park (FWP). NFD operates the low-voltage distribution network, manages electricity retail, and purchases electricity from FWP. FWP sells electricity from onsite renewables, including the three 225kW Vestas V29 turbines, and procures external grid electricity for times of renewables shortfall. This requires contracting with SSEN and a grid energy supply company for distribution and generation to establish tariff rates for site imports and exports [3]. The costs of electricity from onsite renewables and grid imports are passed on to NFD, which adds a small distribution charge as part of the price offered to residents, complicating the state of onsite tariffs.

Interest in Findhorn’s unique energy system has previously led to research collaborations including Orchestration of Renewable Integrated Generation in Neighbourhoods (ORIGIN) and an Energy Technology Partnership (ETP) project with the University of Strathclyde. These projects studied whether demand shifting could reduce carbon emissions by increasing renewables utilisation and will be discussed in the Literature Review. An important legacy of these projects is monitoring and logging of various data of interest through OpenEnergyMonitor Raspberry Pis and the Emoncms web portal.

1.1.1 Woodside Neighborhood

The Woodside neighborhood consists of eight dwellings, half being single-inhabitant studios and other half two-bed homes [4]. Construction concluded in 2022 and tenants moved in thereafter [5]. A district heating scheme with a single 7 kW_e Ochsner Aqua 22 water source heat pump (WSHP) was implemented. Heat pump output cannot be modulated, i.e. it only operates at 7 kW_e. The WSHP separately charges two hot water tanks for space heating (SH) and domestic hot water (DHW) that function as thermal storage [6]. The SH tank is a directly heated 1500 L Akvaterm AKVA1500E [7]. The DHW tank is an indirectly heated 1000 L McCallum Calorifiers Ltd. Stainless Steel Cylinder [8]. During discharging, the SH tank receives return water from the SH loop and the DHW tank receives water from Findhorn's "Living Machine" wastewater treatment facility. Woodside also has approximately 8kW of onsite PV panel capacity. A site schematic is displayed in Figure 1.

The entire Woodside site is extensively monitored and logged, with data recorded for domestic electrical use, thermal storage node temperatures, DHW and SH tank discharge volumes, and other parameters of interest. This data availability makes Woodside an ideal test bed for different heat pump and thermal storage controls.

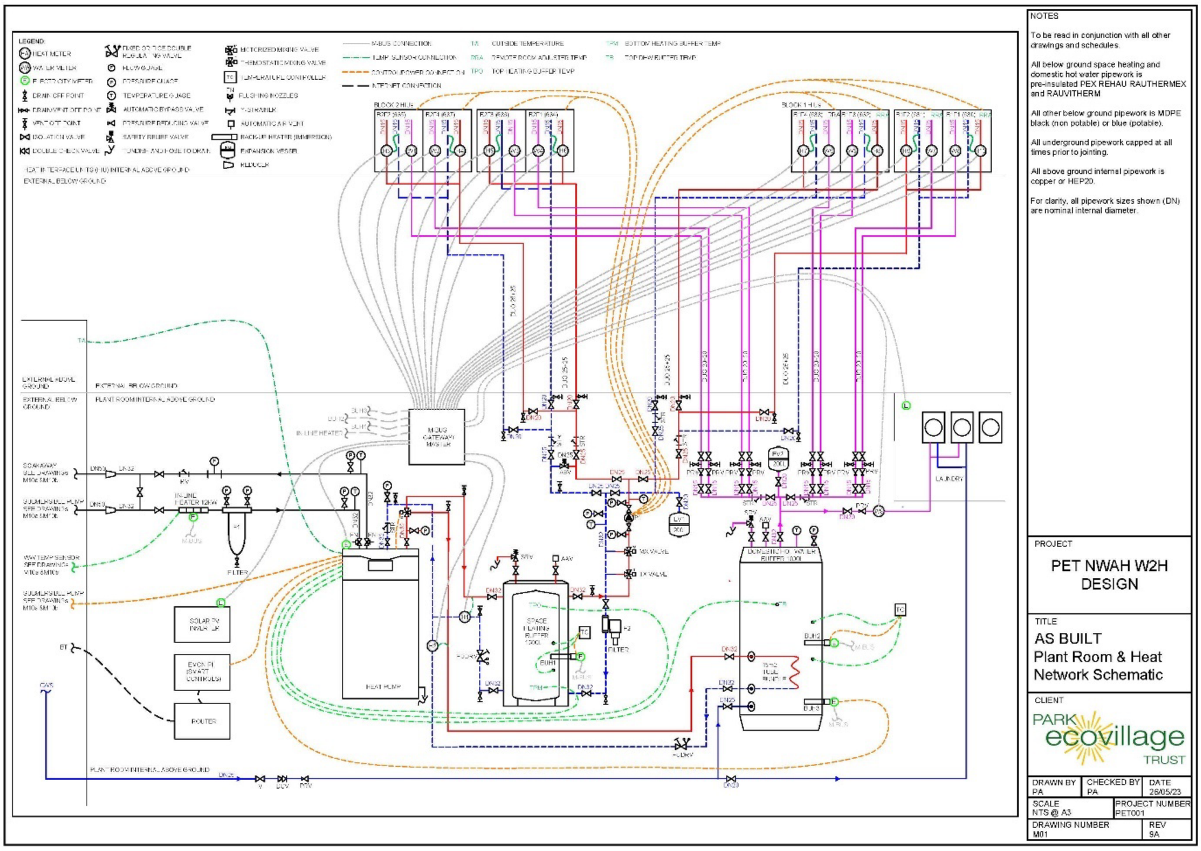

Figure 1. Woodside plant room and heat network schematic [6].

1.2 Problem Definition

Findhorn's energy system poses several challenges. Those addressed in this thesis are electricity supply-demand mismatch, complex grid import contract negotiation, appropriately leveraging onsite data, and incentivizing optimal renewables use.

Findhorn's wind and solar PV assets provide sizable generation capacity, but their variable generation frequently causes a temporal mismatch between supply and site demand. The lack of significant storage assets means that surplus renewables must be exported to a 3rd-party supply company at a low rate, while a shortfall necessitates grid imports that are expensive and potentially carbon intensive. Furthermore, the negotiation process itself is complex and time-limited, making it difficult to assess which contracts are preferable for the entities and residents at Findhorn. Biannual changes in import and export pricing makes it difficult to project the costs of grid imports and plan future electric rates. It is therefore in the financial interest of Findhorn to maximize onsite renewables utilisation through either storage or demand shifting.

Despite the abundance of monitored data available at Woodside and Findhorn, there have been only a few efforts to leverage it for improved system controls. The aforementioned ORIGIN project was the first to show potential benefits, leading to a recent effort to force charging of the DHW tank when solar PV generation exceeded a threshold. However, these controls were only implemented for a short time and did not focus on space heating or wind utilisation. The current controls simply charge the tanks when their top temperatures drop below a threshold, ignoring opportunities for renewables use via forced or delayed charging. This suggests there is scope for more comprehensive controls that better leverage the available site data.

Finally, there is a challenge of incentivizing "optimal" renewables use. The main tool for doing so is electricity tariffs. As Woodside residents own their PV, that electricity is "free" to them, while they must pay the same rate to use NFD electricity regardless of whether Findhorn is currently importing or exporting electricity. This does not appropriately prioritize the use of onsite wind-generated electricity, which is much less expensive than grid imports to NFD (although not free) [9]. NFD has flexibility to set tariffs internally. Therefore, there may be scope to implement different tariffs to incentivize onsite wind use, lowering costs for consumers. However, the magnitude of these benefits and optimal tariff rates are unclear.

1.3 Project Aim and Deliverables

The principal aims of this project are formulated to address the challenges above. They are to:

1) Develop, calibrate, and validate first-principles models for the Woodside DHW and SH thermal storage tanks;
2) simulate Woodside system behavior under different control regimes and tariffs including demand-led rule-based control (RBC), opportunistic PV RBC, and advanced RBC; and
3) compare key performance indicators (KPIs) of operational cost of heat (OCOH), gross annual heating cost, renewables utilisation, and carbon intensity to identify the optimal control scheme and tariff structure.

The primary deliverables of the project shall be documented and validated Python-based tank models, control scripts, and corresponding results for the control and tariff scenarios. It is envisioned that these models and scripts can be adapted for use in other contexts. They are made available on GitHub at https://github.com/eli-d-strath/woodside_control to facilitate this.

The third project aim involves the non-standard KPI of OCOH. OCOH is the total annual cost of electricity used to run the heat pump divided by the total annual thermal energy delivered to homes as space heat or hot water. It is measured in units of £/kWh$_{th}$. OCOH is used instead of levelized cost of heat because the analysis is conducted over a single year and it is assumed no additional capital costs are incurred. Gross annual heating cost represents the total cost of the electricity used to run the heat pump over a year; it has units of £. Renewables utilisation is the percent of electricity used by the heat pump that is generated from onsite PV or wind. Carbon intensity is the average mass of CO_2 equivalents released per kWh of heat energy delivered to residents over the year in units of gCO_2eq/kWh_{th}. Total annual carbon emissions are first calculated assuming intensities of 43, 11.8, and 254 gCO_2eq/kWh_e for solar [10], wind [11], and grid [12] electricity; then, total emissions are divided by the total heat supplied.

1.4 Methodological Approach and Thesis Structure

A methodological project approach was devised to meet the project aims. This approach, outlined below, roughly mirrors the structure of the thesis.

1) Review of Woodside's current energy system and controls.
2) Literature review of options for system modelling, previous research at Findhorn, and research applying control techniques to energy systems.
3) Selection, adaptation, calibration, and validation of tank models.
4) Simulation of all control regimes paired with all tariffs.
5) Analysis of KPIs and graphical representations of system behavior.

The Woodside review provides information for realistic model design and is reflected in Sections 1.1 and 1.2 of the Introduction. The literature review enables an informed modelling approach, suggests where the thesis can build upon previous work, and identifies gaps in the application of controls to thermal storage. This is reflected in Section 2, the Literature and Tools Review. Lessons from the literature review are used to select a modelling approach balancing complexity and accuracy. The PyLESA tank models are then adapted to the Woodside context, addressing Aim 1. This is reflected in Section 3, Thermal Storage Model Development. The models are used to simulate the Woodside heating system as described in Section 4, Woodside Simulation Approach, addressing Aim 2. The KPIs of the simulated scenarios and underlying system behavior are compared in Section 5, Simulation Result Analysis, meeting Aim 3. Finally, an overview of achievements, limitations, and future work is presented in Section 6, Discussion, before a brief conclusion in Section 7, Conclusion.

1.5 Scope and Assumptions

An overview of thesis scope and notable assumptions is provided here. Additional assumptions will be stated throughout the thesis sections and summarized in Section 6.2, Limitations.

The thermal storage models are intended to capture the significant phenomena of charging, discharging, node mixing, and heat loss. The larger Woodside model captures the dynamics of the Ochsner Aqua 22 WSHP, the DHW and SH tanks, and net electricity flow for all of Findhorn. Monthly average water temperatures are considered while calculating WSHP coefficient of performance (COP) and a site energy balance using monitored data is used to determine when wind surpluses occur. The costs mentioned in the analysis refer to the costs directly paid by Woodside residents for electricity used to charge the hot water tanks, without a further breakdown into the costs borne by NFD and FWP.

A detailed analysis of varying losses in the district heat piping system or home internal temperatures and thermal comfort is beyond the scope of this work. However, the demand data used to calibrate and validate the model includes these considerations, so this will not detract from the findings. Site heating demands at each timestep are calculated using monitored volumetric discharge, an assumed flow temperature of 45°C, and assumed tank return temperatures of 10°C and 35°C for DHW and SH. Any required preheating of WSHP inlet wastewater and the scheduled occurrence of tank disinfection cycles are excluded from this analysis. Potential changes in DHW and SH demand and potential effects on the electrical network are not considered. Beyond the whole-site net electrical balance, the rest of Findhorn is beyond the thesis scope.

2.0 Literature and Tools Review

The literature review has three areas of focus: (1) energy system modelling tools, (2) previous research at Findhorn, and (3) previous applications of control to different types of energy systems. Following these sections, identified research gaps relevant to Woodside and the thesis work are summarised.

2.1 Energy System Modelling Tools and Selection Strategy

Tools available for the analysis of local energy systems range from free, open-source tools like OSeMOSYS [13] to advanced commercial tools such as HOMER Pro [14]. They differ dramatically in cost, complexity, features, and customizability. This section reviews tools of potential interest and methods for selecting a tool. It also reviews options specifically for modelling thermal storage.

2.1.1 Tool Selection Methodology

Available models can be categorized in several ways. Després et al. [15] use the flowchart shown in Figure 2, first sorting the tools by availability (open source vs commercial), then by purpose, (large-scale vs local) and finally by approach (bottom-up vs top-down) used by the tool. They then consider how detailed the model resolution is and the specific technologies and economic factors that can be examined. This is useful for categorizing tools but less helpful in selecting tools when several features are desired but unavailable in a single software. Lyden et al. [16] adopt the alternative approach of first marking features as 'essential' or 'desirable' and then scoring a tool's capabilities. This approach allows for a more systematic selection of a software after categorization of the available options.

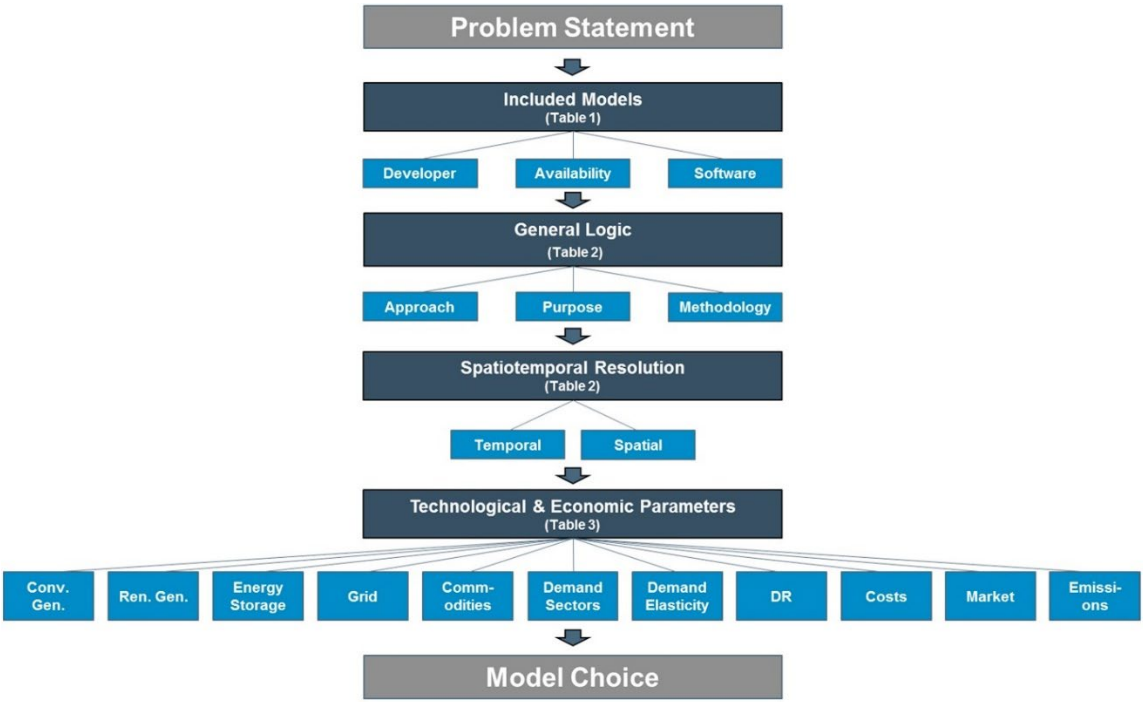

Figure 2. Després et al. energy system model typology [15].

2.1.2 Survey of Available Tools

Numerous tools are available to suit diverse modelling needs. Ringkjøb et al. [17] identify 75 different modelling tools used in the literature after 2012 that are appropriate for systems with high renewable generation shares. A more recent review [18] focused on district heating systems finds 145 modelling tools for local energy systems, identifying 13 as relevant for district systems, while Lyden et al. [16] identify 13 tools relevant for community energy systems with demand-side management. There are 6 tools (DER-CAM, HOMER, EnergyPLAN, energyPro, eTransport, and MARKAL/TIMES) considered tentatively suitable by both [16] and [18]. However, [16] apply their selection process for modelling of a heat pump and thermal storage system at Findhorn and find that only DER-CAM, energyPro, EnergyPLAN, and MARKAL/TIMES meet essential capabilities. Considering the similarity between the Woodside analysis and this hypothetical analysis, these four tools are reviewed further. Python for Local Energy Systems Analysis (PyLESA) [19], an open-source Python tool developed explicitly for the analysis of district heating systems after [16] and [18] were published, is also reviewed. A summary of the tools' attributes relevant to the Woodside context is provided in Table 1.

Table 1. Energy system modelling tools of interest characterized by relevant attributes [16]. DC – demand curtailment, EV – electric vehicles, LS – load shifting, MO – modulating output, NO – non-modulating output, OO – operational optimization with financial (F) or emissions (E) objective function, UO – user-defined order, MPC – model predictive control.

	DER-CAM	*EnergyPLAN*	*energyPro*	*MARKAL/ TIMES*	*PyLESA*
Cost (E)	Free	Free	Paid	Paid	Free
Learning Period (E)	2 days	Two weeks [20]	One day	Months [21]	Minimal
Temporal Resolution (E)	5 minutes	Hourly	Minute	Hourly	Custom
Heat Pump (E)	Y	Y	Y	Y	Y
District Heat (E)	N	Y	Y	N	Y
Availability (D)	Closed source	Semi- open source	Closed source	Open source	Open source
Thermal Storage Model (D)	SSM	SSM	MB	SSM	Multi-node
Financial Analysis (D)	Y	Y	Y	Y	Y
Modelling Approach (D)	Bottom-up optimization	Bottom-up simulation	Top-down simulation	Top-down financial optimization	Bottom-up simulation
Available Controls (D)	DC, EV, LS, MO, OO (F, E)	FO, LS, MO, OO (F)	EV, MO, NO, OO (F), UO	MO, NO, OO (F)	FO, MPC, UO

DER-CAM is a closed-source free tool offered by Lawrence Berkeley National Lab. It is a least-cost or least-carbon optimizer employing mixed-integer linear programming for microgrid systems incorporating distributed energy resources [22]. Its bottom-up approach focuses on economic analysis and has been employed for local energy systems [22].

EnergyPLAN is a free, semi-open-source tool maintained by the Sustainable Energy Planning Research Group at Aalborg University. It models several future systems across energy-related sectors over a year in 1-hour timesteps [23]. It has been widely used in the literature, including for local system analysis, but is intended for modelling at a national or regional scale [24].

energyPro is a closed-source commercial software originally developed for technoeconomic analysis of building energy systems; it has since been applied to local energy projects, particularly combined heat and power (CHP) [25] and district heat systems [26]. Various renewable energy and energy storage technologies can be modelled [27]. Simulations of up to 40 years can be run with 1-minute timesteps.

MARKAL/TIMES is a family of general purpose models developed by the International Energy Agency ETSAP [28]. The GAMS source code is open and freely available, but the GAMS language must be purchased at high cost. They are generally hybrid models that pair top-down economic analysis tools with bottom-up technological models [29]. The models conduct least-cost optimization for multiscale energy systems in the long term and are commonly used at a national or regional level [30], but can be used locally.

Finally, PyLESA is a free, open-source software developed in Python capable of modelling thermal and electrical loads in integrated energy systems [19]. It was designed to address the gaps in modelling tool capabilities identified by [16] including detailed temperature models for thermal storage and adaptable source code. PyLESA considers various renewable energy technologies, heat pumps, thermal storage, electrical storage, tariffs and smart controls [31].

2.1.3 Thermal Storage Models

As flexible charging of thermal storage is the main thrust of this project, thermal storage modelling strategies of the selected tools are examined in greater detail. The physics of hot water tanks are complex, involving various types of heat and mass flow such as conduction, convection, buoyancy, and forced mixing [32]. These produce phenomena such as stratification and thermoclines. Capturing these interactions requires high computational complexity, so many models opt for simplification at the cost of accuracy [32]. A common approach used by industry-standard software such as TRNSYS [33] and academic tools like ESP-r [34] is dynamic thermal simulation. This involves defining system inputs and components and then solving the system iteratively according to thermal and physical rules [35].

The simple storage model (SSM) only measures energy charged in and discharged out of the store, with no analysis of the complex dynamics or temperatures within the store [16]. The SSM is used by EnergyPLAN and the MARKAL/TIMES models. A more complex alternative is the moving boundary model (MB). In MB models, the changing temperatures and masses of two zones with a thermocline between them are considered. No mixing is modelled; instead, the position of the thermocline rises or falls as the tank discharges or charges, respectively [36]. DER-CAM and energyPro employ MB models.

Additional model options, in order of increasing complexity, are plug flow, multi-node, zonal, and computational fluid dynamics (CFD) [32]. Plug flow creates several disks of constant temperature that shift up and down as the tank charges. The disks do not mix, but disks are removed and added to be replaced by new disks of different temperatures. The multi-node approach also considers several disks, but energy transfer is accounted for by changing node temperatures instead of shifting disks up or down [37]. This enables consideration of conductive losses, ambient losses, and enthalpy flow in a single dimension. Modelling with nodes of differing thickness and regression-based heat loss parameters has been demonstrated to reduce the number of nodes needed, reducing computational complexity [38]. The multi-node approach is employed by PyLESA. Zonal models essentially extend the multi-node approach to material and energy balances occurring across three dimensions. This enables better capture of boundary layer flow and jets but comes at a computational cost. CFD offers very accurate analysis but is extremely computationally intensive and is not typically employed in energy system planning models [32]. Figure 3 displays a decision tree for selecting the ideal thermal storage modelling approach considering the available data and accuracy needs.

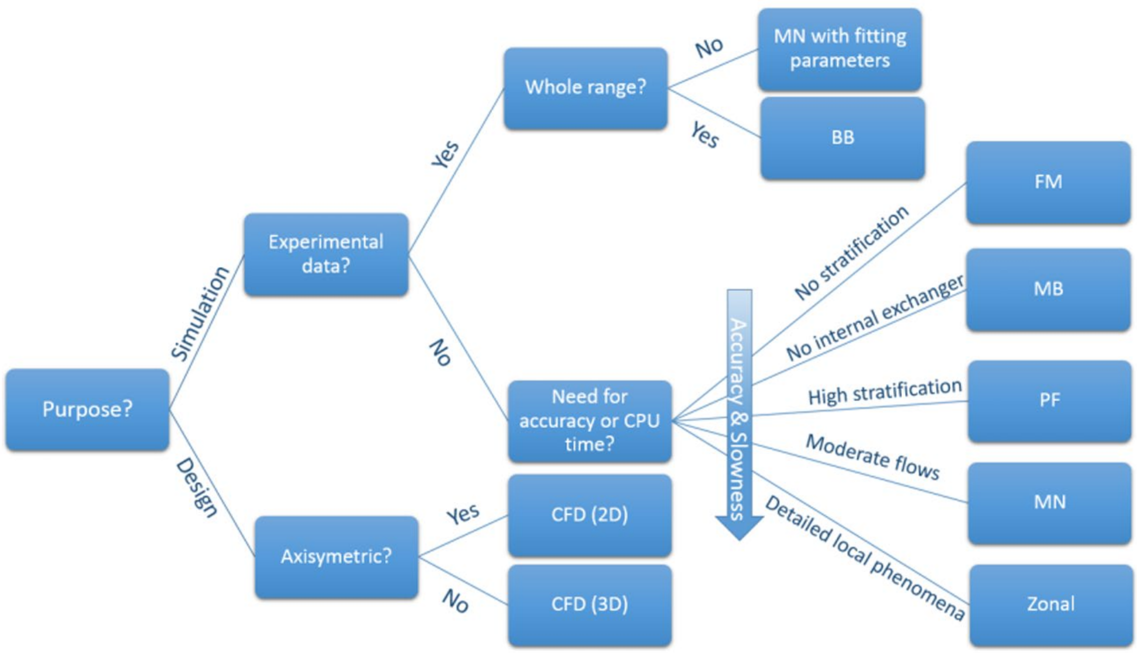

Figure 3. Decision tree for selecting a thermal storage modelling approach from [32].

2.2 Previous research at Findhorn

Findhorn has a history of research collaboration with universities across the UK including the University of Strathclyde [39], [40], Heriot-Watt University [39], and the University of Sussex [41]. This section briefly reviews the research projects previously conducted at Findhorn and their relevance to this thesis work.

2.2.1 ORIGIN

The ORIGIN project was funded by the EU and involved several European universities. It aimed to characterize the electrical and thermal loads of three sustainable communities with local renewables, including Findhorn [42]. This required the installation of monitoring and control equipment throughout the site. Using the information about load and resident behaviour, the project developed an algorithm for demand-side management to increase renewables self-consumption. This algorithm predicted weather, generation, and demand over a 48-hour time horizon and identified opportunities to either charge storage early or defer loads to future periods [39]. After optimizing, a controller then remotely operated heating equipment according to the optimized schedule. Uniquely, ORIGIN attempted to actively engage residents in participatory demand response using dashboards that signalled the current and predicted generation state. This blend of central and user-led load shifting was estimated to increase the use of community renewables by 16% [42].

As part of its characterization of loads, ORIGIN developed thermal models for residential solar thermal storage and a biomass district heat network that were linked to the study's focus buildings [39]. The thermal storage was a physics-based multi-node model with regression parameters to align modelled losses and mixing with observed data as seen in Figure 4.

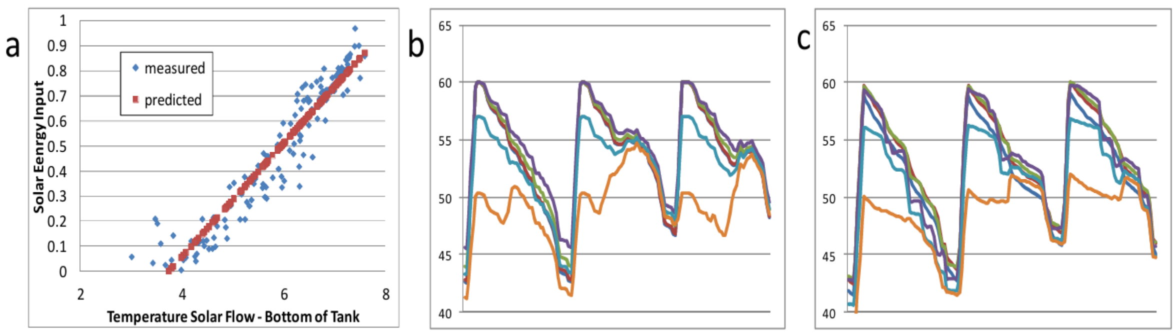

Figure 4. Regression of solar thermal storage tank fitting parameters to improve ORIGIN model prediction, from [39]. (a) Solar Energy Regression; (b) Measured Tank Temperatures; (c) Predicted Performance.

The monitoring kit installed at Findhorn during ORIGIN provides much of the data used to calculate site wind surplus in this thesis. However, ORIGIN thermal modelling is geared towards single-home tanks with low storage capacity (~200-300L). This differs from the needs of Woodside, where the large central district heating network offers increased flex due to the aggregation of demands on a district heating network.

2.2.2 ETPs and SIES

The work during ORIGIN was built upon during an ETP project between NFD, Park Ecovillage Trust (PET) and the University of Strathclyde. This project analyzed a variety of topics at Findhorn including electric vehicles, additional renewable capacity, and energy storage and culminated in Findhorn's 2021 Energy Masterplan [1]. As part of this project, extensive monitoring equipment was installed at the new West Whins development to avoid the challenges faced while retrofitting existing homes during ORIGIN [42]. The PET ETP concluded that batteries or alternative technologies are not economical options for storing surplus generation. However, it built upon ORIGIN's exploratory work leveraging hot water tanks as "thermal batteries" using opportunistic charging and concluded that a 15-20% increase in renewables usage could be attainable [1]. It was suggested that dynamic tariffs similar to Octopus Agile [43], which ties consumer prices to the wholesale rate, could incentivize this opportunistic charging, but a detailed analysis with dynamic tariffs was not conducted.

The initial PET ETP was followed recently by the EU Smart Integrated Energy Systems (SIES) project [44] and Predictive and Opportunistic Control of Renewable Integrated Thermal Stores (POCIT) in partnership with Green Leaf Energy Ltd [45]. SIES and POCIT funded the deployment of detailed monitoring equipment to Woodside and the use of the Emoncms portal, enabling access to node temperature data used for model calibration and validation in Section 3. SIES focuses broadly on virtual power plants and conducted a case study at Woodside assessing the benefits of opportunistic PV charging of the DHW tank. The study found significant cost and renewable usage benefits over a summer week [46]. POCIT complements the SIES project by specifically focusing on developing opportunistic controls for the Woodside heating system as a lesson for use in the rest of Findhorn [45]. POCIT efforts inform the work conducted in this thesis.

2.3 Control Techniques Applied to Energy Systems

This subsection examines the motivation behind controls for energy systems and briefly surveys the literature of controls applied to energy systems. Examples of interest are presented.

2.3.1 Motivations for Control

Controls are essential for energy systems, as they have inherently high complexity due to the number of associated factors. Depending on the scale of the system in question, these factors can include mechanical equipment, electrical equipment, generators, distribution lines, chemical storage, and stochastic variables like weather and human input [47]. Energy systems have traditionally accepted demands as fixed inputs and orchestrated supply to meet these demands. In this paradigm, controls are used to most efficiently schedule generation and maximize system performance or minimize cost. They are also used in power systems engineering to ensure system reliability [48] and prevent service interruptions [49]

The relationship between supply, demand, and controls is shifting as variable renewable energy (VRE) becomes more prevalent [50]. VRE generation can be predicted in the short term but is not dispatchable. Conversely, VRE sources may generate at times of low demand and need to be curtailed, wasting cheap energy. In this emerging context, detailed monitoring and controls are increasingly required to shift demand to times of VRE generation [51], [52], [53]. Thus, a major goal of advanced controls is enabling optimal renewables utilization while maintaining or improving system performance, such as providing heating for thermal comfort.

2.3.2 Controls Applied to Building Electrical Demands

A subsector of the energy industry that has traditionally used controls is building energy management systems (BEMS). BEMS are a general category of management tools that operate heating, ventilation and air conditioning (HVAC) systems that modulate internal building conditions to promote thermal comfort and health [54]. The BEMS is tasked with using monitored information such as temperature and weather prediction to efficiently operate these HVAC systems and minimize energy losses. A variety of control and optimization strategies have been deployed to achieve these aims in the context of large commercial buildings [55]. These can be broadly classified as rule-based controls and predictive controls. RBC involves a set of rules that are assessed at each timestep. If current conditions violate the rules, the BEMS acts to rectify this violation. Conversely, predictive controls estimate future conditions such as energy demands and weather and adjust the kit they control to optimize system operation with these predictions in mind [56].

BEMS are increasingly being applied to more complex contexts with renewable generation and other technologies. Chellaswamy et al. [57] apply a BEMS predictive control methodology to a residence with solar PV to efficiently utilize the PV generation for domestic needs. Gao et al. [58] develop a hybrid BEMS MPC approach and use it to optimize the operation of solar PV and a battery considering both safety metrics and costs. Srithapon and Månsson [59] find that costs can be reduced by applying MPC within a domestic BEMS to coordinate electric vehicle charging with thermal demands that are met via thermal storage and a heat pump. Abushnaf et al. [60] develop a BEMS that controls household appliances and assess its performance under time-of-use, inclining block rate, and real-time pricing tariffs. Other studies [61] have been conducted with BEMS to manage domestic electricity use, but these applications are restricted to management of individual homes and focus on electrical loads over thermal loads.

2.3.3 Controls Applied to District Heating Networks

BEMS has been extended to district heating networks, which are of particular interest for this thesis. [56] analyze a district heating system where residents can both contribute to and draw heat from a central thermal store. However, the sources of heat in this system are boilers or solar thermal collectors as opposed to the WSHP at Woodside. Behzadi and Sadrizabeh [62] developed a BEMS with TRNSYS and rule-based controls that are optimized using machine learning. This control system is applied to a dual network comprised of a district heat network and electrical assets for hydrogen generation. Although the model includes a hot water tank, the primary focus of analysis is the generation and use of hydrogen to provide heat. Kuosa et al. [63] take the novel approach of directly using a district heating pipe network as a storage asset by charging at heightened temperatures during periods dictated by a controller. They achieve significant reductions in backup heating use and carbon emissions. While intriguing, this is not a desirable strategy at Woodside because the hot water tank capacity is far greater than the district heat pipe capacity. Hassan et al.'s [64] optimization of thermal energy storage operation within a district heating scheme more closely resembles the Woodside context, as a stratified hot water tank is used. However, the district heating scheme is charged using a biomass boiler and backup electrical heating, not a heat pump. This review indicates that there is a lack of research on district heating systems with thermal energy storage that are charged solely by heat pumps.

2.3.4 *Wind to Heat Controls*

The large wind generation capacity at Findhorn Ecovillage makes wind-based controls particularly appealing. Recent work by Desguer et al. [65] analyzes the potential use of thermal storage in electrified district heating systems to mitigate wind power curtailment. Their case study finds that a district heating system can operate almost entirely on wind power that is otherwise curtailed, but that appropriately designed markets are necessary to achieve this level of wind-driven charging. While the Woodside current context differs in that surplus wind generation is exported at a flat rate, not curtailed, this situation may change in the future. Third-party brokers may become unwilling to purchase surplus electricity at times when wind generation in nearby locations is also high, leading to loss of value to Findhorn. Opportunistically charging thermal storage at Woodside and other locations then offers a way to recover value while cheaply providing heat, though it is unclear whether the existing thermal storage capacity approaches levels sufficient to capture significant amounts of surplus wind. The Desguer et al study [65] suggests that alternative tariffs may be required at Findhorn to incentivize use of wind power for charging the Woodside thermal storage.

2.4 Identified Research Gaps

Previous research at Findhorn established a rich monitoring infrastructure and examined the potential for load shifting using residential thermal storage. Though comprehensive, these efforts did not examine the Woodside district heating system because it did not yet exist. Recent efforts associated with SIES assessed the cost savings from implementing opportunistic PV charging of the DHW tank at Woodside. However, the SIES analysis did not examine opportunistic wind charging or charging of the SH tank. There is ample research applying BEMS to optimize domestic and community electrical consumption, but less research analyzing district heating schemes. No studies could be identified that analyzed district heating schemes incorporating hot water tank-based thermal storage charged using a heat pump.

This thesis addresses the gaps in general energy systems modelling and research conducted at Findhorn. The contents build directly upon ORIGIN, SIES and POCIT in two ways. First, this project leverages data from monitoring equipment installed for these projects. Second, this project extends the controls proposed in SIES and POCIT to a novel context by simulating with detailed multi-node tank models, applying controls to both the DHW and SH tanks, and simulating operation with dynamic tariffs.

3.0 Thermal Storage Model Development

To model the Woodside energy system, the multi-node thermal storage model developed as part of PyLESA was extracted and modified. Separate control scripts that simulate the remainder of the system were then written in Python. This section provides a rationale for this approach considering the available tools reviewed in subsection 2.1, further details the multi-node model used in PyLESA, and explains what modifications were made to the model. Finally, model validation was conducted using monitored site data and simple controls reflecting the current demand-led control paradigm.

3.1 Modelling Tool Selection

This subsection justifies the choice to use the dedicated PyLESA thermal storage model in tandem with novel simulation and control scripts instead of the available software mentioned in subsection 2.1. The modelling tool attributes that were essential and desirable for the project were identified. The tools reviewed in subsection 2.1 were marked against these requirements following the selection methodology described in [16].

Table 2. Energy modelling tool marking against essential (E) and desirable (D) attributes based on [12]

	DER-CAM	*EnergyPLAN*	*energyPro*	*MARKAL/ TIMES*	*PyLESA*
Essential Capabilities	**Fail**	**Fail**	**Fail**	**Fail**	**Pass**
Total Score	**11**	**10**	**10**	**6**	**14**
Cost (E)	2	2	0	0	2
Short learning period (E)	2	0	2	0	2
Sub-hour Resolution (E)	2	2	2	2	2
Heat Pump (E)	2	2	2	2	2
District Heat (E)	0	2	2	0	2
Availability (D)	1	0	0	1	1
Advanced Thermal Storage (D)	0	0	1	0	1
Financial Analysis (D)	1	1	1	1	1
Bottom-Up Model (D)	1	1	0	0	1
Predictive Controls (D)	1	1	0	0	1

The scoring and marks are indicated in Table 2. The project budget and time constraints made a low-cost (preferably free) and easily learned tool critical. Sub-hourly resolution was necessary to best utilize the onsite data and accurately model a system with variable heating demands and renewable generation [66]. Finally, district heat and heat pump modelling capabilities were considered essential, as these are defining qualities of the Woodside energy system. Attributes that were desirable but not essential included an advanced thermal storage model for accurate simulation of the temperatures and useful available energy in the thermal stores. Open-source code enables customization, which was desirable because the Woodside heating system is unique and likely required adjustment of native capabilities. It also promotes transparency and enables future improvement of this work [67]. A bottom-up approach with financial analysis was desired because it enabled technically detailed modelling and produced the financial outputs that are key for decisionmakers at Findhorn.

This marking process eliminated all modelling options except PyLESA. MARKAL/TIMES cost several thousand pounds, required extensive training, and did not have district heat modelling capability. energyPro was also expensive, though it met other needs and could be explored for similar future projects if low-cost licenses could be obtained. EnergyPLAN was free but not fully open source and required a long training period. DER-CAM was accessible and open source but did not have district heating capability. Beyond satisfying essential capabilities, PyLESA also had an advanced thermal storage model and offered a bottom-up approach with financial analysis. Because it was written in Python a variety of libraries [68] created to work with energy systems could also be imported and applied, if necessary.

The entire PyLESA software package offered various capabilities that exceeded the needs of the current project. These included renewable generation estimators, demand generators, and a detailed tariff assessment tool [19]. Additionally, PyLESA only modeled a single thermal storage tank that assumeed direct water charging; this was problematic because the DHW and SH tanks at Woodside were separate and heated differently. Therefore, this project used the multi-node tank model module from PyLESA as the basis for developing Woodside-specific DHW and SH thermal storage models. The contents of the heat pump module were also adapted for heat pump modelling within the control scripts. Extracting the essential aspects of the PyLESA tool reduced computational burden while maintaining the advantages of being freely available, open source, and thermally detailed.

3.2 PyLESA Thermal Storage Model

This subsection briefly reviews the PyLESA thermal storage model, underlying assumptions, and its validation.

3.2.1 Model Approach

PyLESA used a first-principles multi-node (MN) thermal storage model [19]. The MN approach could track node temperatures and considered phenomena such as internal conduction, node mixing, and ambient heat loss [32]. Tracking node temperature, not just state of charge, was important to ensure that tank outlet temperatures at the top node were sufficient for domestic hot water and space heating. MN had a far lower computational cost than other approaches with temperature tracking such as a zonal model or CFD [32].

The MN approach employed by PyLESA divided the tank into nodes of equal mass and applies material and energy balances to compute temperature changes across model timesteps. PyLESA's balances accounted for ambient heat loss to the tank surroundings; flow during tank charging; flow during tank discharging; and mixing of the node masses [69]. Ambient losses included conductive losses through the cylinder and connection losses through insulation openings. The connection losses were calculated depending on insulation k-value and ambient air temperature. Mass flowed into the top of the tank during charging and out of the bottom node. Mass flowed into the bottom of the tank during discharging and out of the top node. The direction of node mixing was determined by the tank state, with downwards mixing during charging and upward mixing during discharging. When the tank was on standby, no mixing was calculated. These flows of energy and mass are shown in Figure 5.

An overall energy balance for the currently analyzed node *i* was developed considering these terms and shown in Equation 1.

Equation 1. Overall energy balance for node i *in PyLESA thermal storage model. m_x – mass flow in x direction; cp – heat capacity of water; T_x – temperature at node or source x; F_c – function of charging (0 or 1); F_d – function of discharging (0 or 1); F_e – empirical overall correction factor; F_{corr} – empirical insulation correction factor; k – insulation k-value; r_1 – internal tank radius; ; r_2 – external tank radius; h – node height; c.l. – connection losses [69].*

$$\left(m_i c_p\right)\frac{dT_i}{dt} = F_c \dot{m}_{in} c_p T_{in} - F_d \dot{m}_{out} c_p T_i + F_c \dot{m}_{down} c_p T_{i-1} - F_d \dot{m}_{up} c_p T_i - \tag{1}$$

$$F_c \dot{m}_{down} c_p T_i + F_d \dot{m}_{up} c_p T_{i+1} - F_e \left[F_{corr} k \left[\frac{T_i - T_0}{r_2 - r_1}\right] \pi\left[r_1^2 + h(r_2 + r_1)\right] + c.l.\right]\left(m_i c_p\right)$$

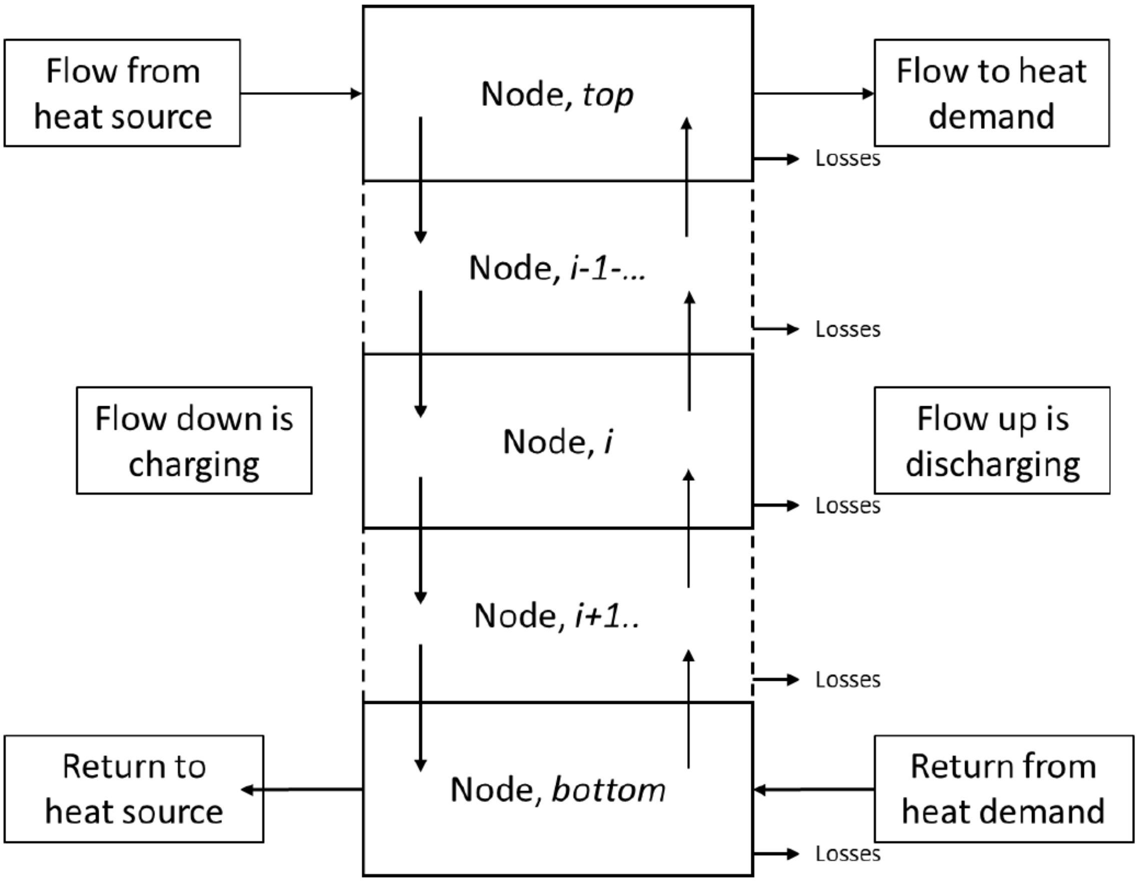

Figure 5. Schematic of the energy and mass flows accounted for in the PyLESA thermal storage model [69].

Equation (1) was simplified by sorting terms into those dependent on the current node temperature (T_i), above node temperature (T_{i-1}), below node temperature (T_{i+1}), and no node temperature, assuming nodes are numbered from the top. These were represented by the coefficients A, B, C, and D, respectively. During each model timestep, the tank underwent N (number of nodes) internal timesteps in case the desired charge or discharge mass exceeded that of the nodes. Node coefficients were calculated at each timestep and the change in node temperature was computed with an ordinary differential equation solver in the SciPy library [70]. New node temperatures were then produced and used for the subsequent model timestep.

The model took inputs of tank capacity, insulation type, number of modelled nodes, and insulation thickness. Five nodes were used by default. Additional inputs included the number of tank openings and connections; the size of these openings; and empirical correction factors for flaws in insulation and any necessary overall adjustments to heat loss. Using a preset factor, model width and height were calculated relative to tank capacity. The tank internal radius was calculated assuming insulation was internal to the calculated tank width.

This tank model was implemented in Python using an object-oriented approach. A Hot Water Tank class was defined with numerous internal methods to carry out the node temperature update process and methods that are called in the main operation script. For a more detailed description of the thermal tank model and its implementation in Python, refer to [69] and [19].

3.2.2 Assumptions

The assumptions underlying the PyLESA thermal storage model are listed below.

- The tank was a perfect cylinder
- Heat transfer occurred only through side and top/bottom walls, not corners
- Insulation provided the only thermal resistance between the tank and ambient air
- The tank was at steady state conditions
- Node mixing did not occur when tank was in standby mode
- Turbulent effects were not considered
- Tank charging inlet and discharging outlet were in the top node
- Return water outlet and inlet were in the bottom node

3.2.3 Validation

Validation was conducted by comparing modelled node temperatures to monitored data for a district heat system over a charging period, discharging period, and period of mixed operation. This comparison indicated that the time taken for complete tank charging is accurate, but that the model misses some aspects of stratification, as it simulates node temperatures increasing evenly instead of sequentially and rapidly [69]. The observed mean absolute error (MAE) and mean absolute percentage error (MAPE) were greatest for the bottom node during charging due to accelerated node mixing caused by internal tank timesteps. The discharging validation similarly showed more gradual simulated node temperature declines compared to monitored data. Over a two-day period the simulated tank node temperatures roughly followed the pattern of observed data with an MAE of 2.5°C and maximum error of 12°C [69]. This was taken to indicate that the model could not precisely predict node temperatures at each timestep, but could realistically reproduce general charging/discharging behavior and temperature changes.

3.3 Model Adaptations for Woodside

This subsection discusses the modifications made to the PyLESA thermal storage model to produce useful models of the Woodside DHW and SH tanks. Graeme Flett made preliminary changes to produce distinct DHW and SH tank models, but these models were not fully documented or validated. This thesis thoroughly documented the Flett models and used them as a starting point for additional changes. The initial changes by Flett and later changes for this thesis are introduced and discussed. The original PyLESA model is referred to as the base model; the preliminary models are referred to as the Flett DHW and SH models; and the models produced during the thesis work are referred to as the thesis DHW and SH models.

3.3.1 Domestic Hot Water

The changes introduced to the base model to produce the Flett DHW model were uneven node masses; direct use of volumetric demand data as the tank discharge mass; and an empirical calculation of heat loss. [32] indicated that using uneven nodes could reduce the number of nodes needed to capture phenomena like thermoclines. In the Flett DHW model, more node mass were assigned to the bottom node than the top, while the middle nodes were assigned a mass between the top and bottom node mass. The empirical heat loss model was derived from tank temperature data during periods without charge or discharge. It involved a heat loss factor specified for each node that was used to calculate coefficients A and D. This approach to heat loss was like that used in ORIGIN [39]

The changes introduced to the Flett DHW model to produce the thesis DHW model were altering the approach to charging and node mixing; using a 0.66 scaling factor for the calculated discharging mass; changing the assumed return temperature to 10°C; and calibrating node mass and heat loss factors. The Flett model maintained that charging water enters the top node and drives downward mass and energy flow, with water leaving the bottom node to return to the heat pump. However, the actual Woodside DHW thermal storage is indirectly charged midway down the tank. The model of tank charging and node mixing was altered to address this as shown in Figure 6. In the thesis DHW model, charging water entered the 4th node down from the top. All nodes above the charging node received water from below while sending an equivalent mass of water in the opposite direction. Finally, the charging node sent a mass equivalent to the charging mass "out" of the tank, simulating the function of the heat exchanger. The bottom node therefore did not directly mix or interact with any other nodes and was assigned a small share of the total tank mass. The 0.66 scaling factor was introduced because the calculated tank energy loss, as calculated by a change in node temperature, was consistently greater than the calculated discharge energy by a factor of ~1.5. A return temperature of 10°C more accurately reflects the water temperatures coming from the Living Machine to the tank during discharging. The final DHW tank model had node masses of [150, 200, 250, 275, 125] kg. Empirical heat transfer coefficients of [2.5, 2.0, 2.5, 8, 30] were used, reflecting the bottom node's sensitivity to ambient conditions because it is not directly charged or mixed with the other nodes. The thesis DHW model used the same discharging approach as the Flett DHW model and base model.

An alternative discharging approach, in which mass flows solely upwards and "out" of the tank at the top node, was considered and analyzed. However, validation attempts revealed poor alignment between model and monitored node temperatures. The first approach for modified charging and mixing was therefore implemented.

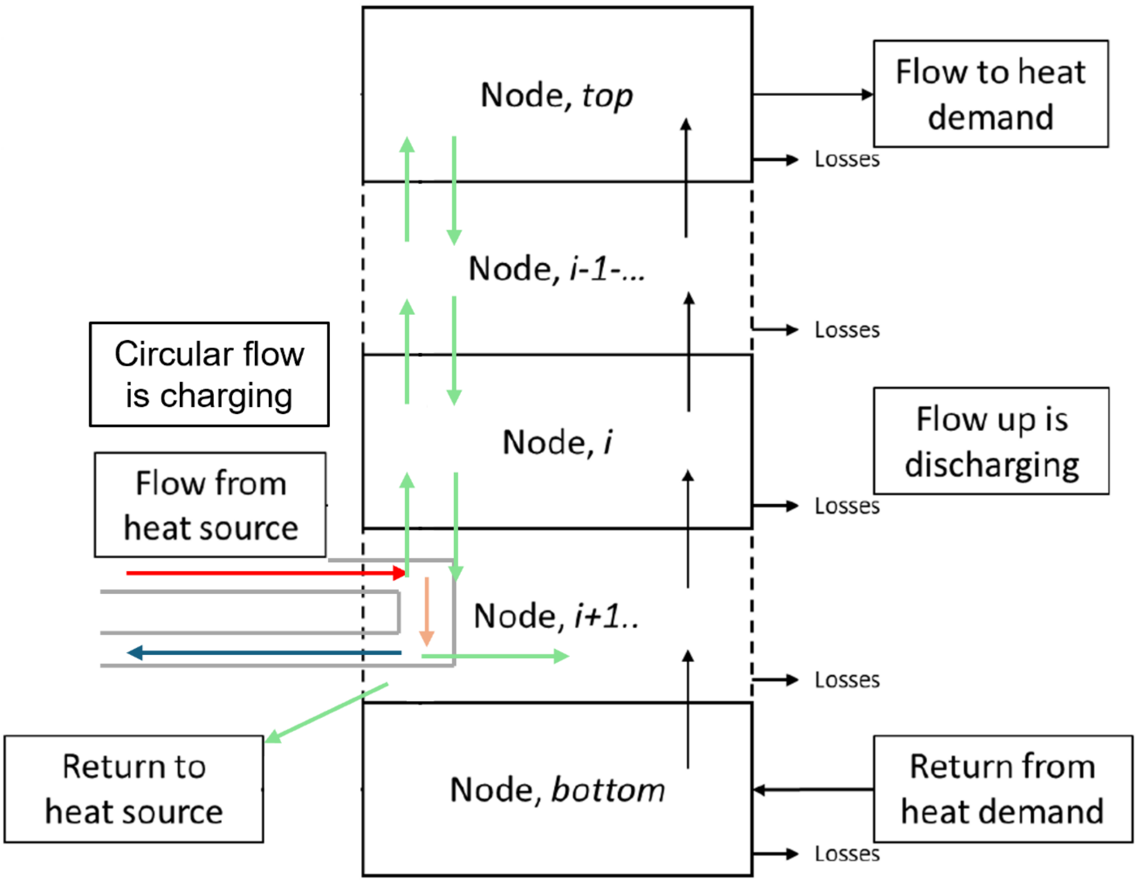

Figure 6. Schematic of the energy and mass flows in the modified Woodside DHW thermal storage model, based on [69].

3.3.2 Space Heating

The sole initial change to create a Woodside SH model was the introduction of uneven node masses, with more mass in the upper nodes. As mentioned, this can improve the ability of the model to capture thermoclines and stratification effects [32]. The focus of Graeme Flett's previous work was forced DHW charging, explaining the lack of changes to the SH model.

The SH model implemented the energy and mass flow approach found in the native PyLESA model as described in Figure 4. Accordingly, the overall model was first principles based with empirical adjustment to improve alignment with monitored node temperatures. The final SH tank model has node masses of [300, 250, 250, 300, 400] kg.

3.4 Model Calibration and Validation

This subsection discusses the calibration and validation of the modified thermal storage models. Simulated DHW and SH tank node temperatures were validated against monitored Emoncms node temperature data between November 1 to November 14, 2023. Various versions of the model were assessed to identify suitable node masses and, for the DHW tank, empirical heat loss factors. Only the final models are discussed. The standard statistical metrics of MAE, MAPE [71], and CVRMSE [72] alongside visual methods were used to assess how well the model corresponds to monitored data and charging/discharging trends.

3.4.1 Domestic Hot Water

The final DHW tank model had node masses of [150, 200, 250, 275, 125] kg from top to bottom. The empirical heat transfer coefficients used were [2.5, 2.0, 2.5, 8, 30], reflecting the bottom node's sensitivity to ambient conditions because it did not directly charged or mixed with the other nodes. The calibration graphs for each node temperature are shown in Appendix 1 (Figures 15-19).

Calculated node temperatures above the heat pump source temperature (51°C) were set back to the source temperature, with the "lost" energy resulting from the temperature decrease transferred to the node below. The basic demand-led controls triggered charging when the 3rd node temperature dropped below 46°C and stopped charging when the top node temperature exceeded 50.5°C. These values were selected based on observed patterns in the monitored data. MAE, MAPE, CV RMSE, and maximum error of the modelled vs monitored node temperatures over the 672 half-hourly validation timesteps are presented in Table 3. Nodes 1 and 2 display low MAE, MAPE, and CV RMSE, indicating accurate modelling of these temperatures. Node 3 values are acceptably accurate, while Node 4 and 5 temperatures are less accurate as indicated by the large MAE, MAPE, and CVRMSE.

Table 3. Statistical outputs of DHW tank model validation against monitored node temperature data.

	Node 1 (Top)	*Node 2*	*Node 3*	*Node 4*	*Node 5 (Bottom)*	*Average*
MAE [°C]	0.70	0.71	1.55	6.04	4.92	2.78
MAPE	1.42%	1.45%	3.17%	16.63%	32.12%	10.96%
CVRMSE	2.01%	2.04%	4.14%	19.02%	32.00%	11.84%
Maximum error [°C]	3.30	3.70	10.20	22.18	8.40	9.56

The graphical representation of the first 96 validation timesteps in Figure 7 gives context to these statistical findings. This period included charging, standby, and discharging periods. Model temperatures closely followed monitored temperatures for the first two nodes across charging and discharging periods. The third nodes charged to the expected maximum temperature, but its temperature dropped more rapidly than the monitored temperature during discharging periods. As the controlling node, this meant charging cycles were initiated at different timesteps than in the monitored data. Node 4 model temperatures did not always reach the expected maximum during charging, but dropped less during discharge periods, accounting for the large maximum error, MAE, and MAPE. This charging behavior can be attributed to the use of a mass flow "exiting" the charging node in the model to maintain steady-state tank mass. Future analyses may wish to explore a scaling coefficient to reduce the magnitude of this energy loss. The large error is magnified by the temporal mismatch in charging cycles. Node 5 shows an inverse relationship in which modelled temperatures exceed monitored temperatures, which may be caused by poor capture of stratification [69].

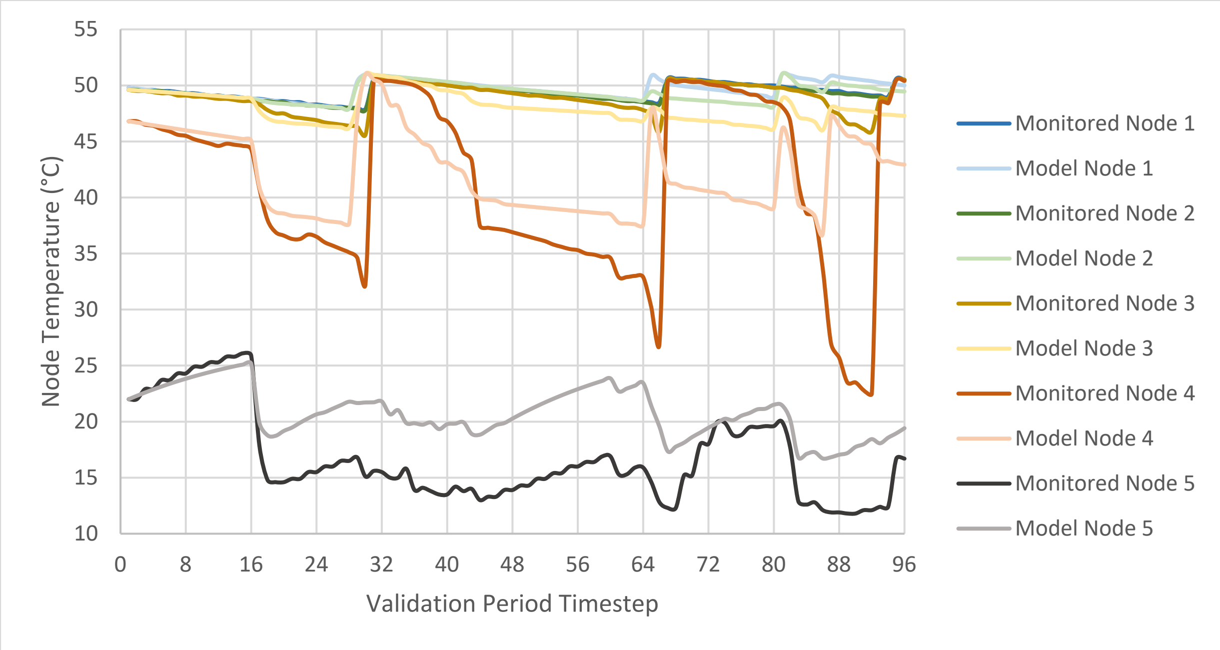

Figure 7. Modelled and monitored DHW tank node temperatures across the first 96 validation timesteps

The DHW model's average MAE of 2.78°C and MAPE of 10.96%, as well as 3°C+ maximum error for each node, indicate it is not appropriate for precise tracking of node temperatures. However, the top three nodes are adequately tracked, which is most relevant for the purposes of approximating when charging will occur and whether the top node is able to meet demand at the required outlet flow temperature. Worse tracking of lower node temperatures is commonly seen and associated with imperfect capture of stratification and the movement of the thermocline [19]. Furthermore, the average CVRMSE of 11.84% falls below the 20% threshold in ASHRAE Guideline 14 to consider a model calibrated [72] and the general charge-discharge dynamics of a thermal store are captured. Taken together, the validation indicates the thesis DHW model is suitable as a basis for system analysis.

3.4.2 Space Heating

The final SH tank model has node masses of [300, 250, 250, 300, 400] kg from top to bottom. Only top and bottom node temperature data is available for the SH tank in the Emoncms portal. This limits validation and analysis to these nodes and restricts control options. However, the model is still run with five nodes. Basic demand-led controls trigger charging when the top node temperature drops below 50°C and stop charging when the top node temperature exceeds 56°C. This approach is based on observed patterns in monitored data; however, temperature data occasionally show charging at different threshold temperatures. The exact details of onsite controls used at this time are unavailable, so the stated approximation is made. MAE, MAPE, CVRMSE and maximum error of the modelled vs monitored node temperatures over the 672 half-hourly validation timesteps are presented in Table 4.

Table 4. Statistical outputs of SH tank model validation against monitored node temperature data.

	Node 1 (Top)	***Node 5 (Bottom)***	***Average***
MAE [°C]	1.64	8.52	5.08
MAPE	3.07%	17.72%	10.40%
CVRMSE	3.92%	20.69%	12.31%
Maximum error [°C]	7.46	17.46	12.46

Node 1 has low error across metrics, indicating the model accurately tracked Node 1 temperatures. However, Node 5's high error suggested it was poorly tracked. The validation of the DHW model suggested that intermediate nodes would have lower error than the bottom node. Therefore, the lack of available data from temperature sensors midway along the tank for comparison with model node temperatures was likely to inflate the average MAE and MAPE.

A graphical representation of the first 96 validation timesteps encompassing charging standby, and discharging periods is shown in Figure 8. Modelled temperatures for intermediate nodes were included for completeness. There is an inconsistent relationship between modelled and monitored node temperatures during discharging; at times the modelled temperatures decreased more slowly, at others more rapidly. This caused more frequent charging in the model. The selection of node masses in the model may be responsible, although the behavior was observed across a suite of tested node mass distributions. Furthermore, monitored temperatures for the bottom node were significantly higher than modelled temperatures after charging. This suggests that the magnitude of node mixing between the top and bottom of the tank is unaccounted for in the model. The general cycle of node temperatures rising and falling during charging and discharging is observed and no node temperature inversions occur.

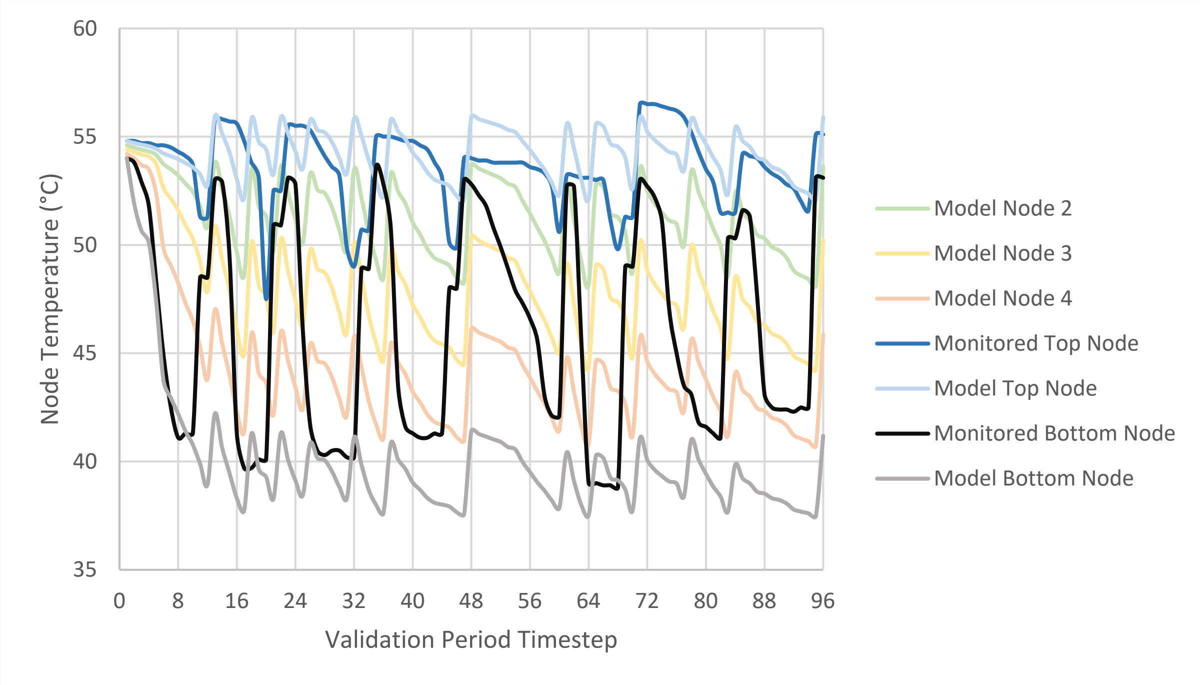

Figure 8. Modelled and monitored SH tank node temperatures across the first 96 validation timesteps.

Like the DHW model, the average MAE of 5.08°C, MAPE of 10.40%, and maximum errors exceeding 7°C indicate the model does not precisely track node temperatures. The graphical analysis corroborates this assessment and demonstrates that the precise timing of charging events differs. However, the average CVRMSE of 12.31% is below the standard calibration threshold of 20% [72], the top node temperature is well tracked, and the expected charge-discharge trends are observed. These validation results suggest the modified SH model is suitable for the purposes of this analysis.

4.0 Woodside Simulation Approach

This section describes the simulation of the Woodside heating system over a full year in half-hourly timesteps. The site demand and generation data used during simulation and methods for data preprocessing are discussed. The selected simulation approach is then introduced. To conclude, the control regimes and tariffs examined during simulation are listed and explained.

4.1 Data Sources and Cleaning

This subsection reviews the sources of heat and electrical demand data for Findhorn and the steps taken to process this data.

Several datasets were used during simulation of the Woodside heating system. These included onsite PV generation; SH and DHW volumetric demand; daily average air temperature; and net power draw from West Whins, the wind turbines, and the rest of Findhorn. The datasets covered the period from January 1, 2023, to December 31, 2023. Monitoring gaps present in some datasets during this period were addressed using synthetic data. Datasets were created by aggregating Emoncms data reported in 10-seconds intervals into half-hourly values. These represented either a sum for energy and volume units or an average for power units. Table 5 reviews the source of these datasets, their level of resolution, and whether they contain only monitored data or are a hybrid of monitored and synthetic data.

Table 5. Datasets used in simulation described by source, temporal resolution, and naturalness of data.

Dataset	*Source*	*Resolution*	*Data Type*
PV Generation [kWh]	Emoncms	Hourly	Monitored
DHW Demand [L]	Emoncms	Hourly	Monitored
SH Demand [L]	Emoncms	Hourly	Monitored
West Whins-Southside Active Power [kW]	Emoncms	Hourly	Hybrid
CB001 Active Power (Wind) [kW]	Emoncms	Hourly	Hybrid
CB002 Active Power (Findhorn) [kW]	Emoncms	Hourly	Hybrid
Daily Ambient Temperatures [°C]	Kinloss Met Office [73]	Daily	Monitored

Generation data for the Woodside PV panels, DHW volumetric demand, and SH volumetric demand were obtained from Emoncms and aggregated to half-hourly values. Daily ambient temperatures measured at the nearby Kinloss Met Office were obtained via their website [73]. The West Whins-Southside (WW-SS), CB001, and CB002 feeds monitor nearly all the sites at Findhorn, including the FWP turbines, distributed PV, commercial buildings, and residences. Therefore, it was assumed that the balance of these streams represents net onsite consumption and indicates when a renewable surplus occurs. These datasets were partially synthetic due to a lack of continuous monitoring during 2023. Electrical demand was only monitored at WWSS during the last 3 months of 2023; therefore, the first half of the dataset was filled with monitored 2024 data, with the remaining gap filled by repeating the demand values from the end of 2023. The CB001 and CB002 feeds contained three gaps in monitoring from half-hourly timesteps 1 to 1374, 2899 to 3582, and 6217 to 6798. These recording gaps totalling approximately 55 days were filled with 2024 electrical feed data.

The decision was made to integrate 2024 into 2023 data gaps because it was assumed that monitored data, regardless of year, was more accurate than generated load profiles. This was justified by a lack of notable changes to the Findhorn site from 2023 to 2024 and relative consistency in year-to-year user electrical demand behavior. Any discrepancies caused, for example, by extended cold snaps in one year will have a small effect on results, as the WWSS feed is much smaller in magnitude than CB001 and CB002, and only 15% of timesteps were filled with 2024 data for CB001 and CB002.

These streams were cleaned by the control scripts as they are read in to remove any sensing errors giving extreme positive or negative values. Particularly, DHW and SH volumetric demand that was negative or exceeded 500 L was set to 0, as were negative values for Woodside PV. Net site renewable power was capped at 750 kW and negative values were set to 0. The cleaned DHW and SH volumetric demand data were then used to calculate heating energy demand as shown in Equation 2. A 45°C flow temperature was assumed for both the DHW and SH tanks. Return temperatures of 10°C and 35°C were assumed for the DHW and SH tanks, respectively. The 45°C DHW flow temperature was assumed because DHW delivery temperature typically varies between 35 and 46°C [74] in real systems. The Woodside DHW tank also lacks a mixing valve, so temperatures above 46°C run the risk of scalding residents. The 10°C DHW return temperature was based on the assumed temperature of water in the

Living Machine wastewater treatment facility that replenishes the DHW tank. The 45°C SH flow temperature and 35°C return temperature were selected based on the Flett controls to mirror the current system.

Equation 2. Calculating timestep heat demand from volumetric demand. Q – heat energy; V – volume demand in timestep; C_p – water specific heat of 4.181 kJ/kg-[redacted]ΔK; ΔT – difference between flow and return temperatures.

$$Q = V * C_p * \Delta T \tag{2}$$

4.2 Simulation Approach

This subsection outlines the approach to simulate Woodside heating system operation over the 2023 calendar year. Python files that declared a control-specific class, *demand_led_rbc.py, opp_pv_rbc*, and *advanced_rbc*, were written for each of the three controls. A *main*.py control script was written that instantiated these classes and executed model simulation. Two additional scripts, *sim_tools.py* and *result_tools.py*, contained methods used during simulation or results outputs. Each of the four control approaches (described in Section 4.3) was simulated with all five tariff structures (described in Section 4.4) for a total of twenty scenarios.

This project simulated over a 365-day period with half-hour timesteps. Control values were specified in accordance with those used in Section 3.4. Briefly, minimum top node temperatures of 46°C and 50°C, maximum top node temperatures of 50.5°C and 56°C, and heat pump source temperatures of 51°C and 57°C were used for DHW and SH, respectively. During opportunistic renewable charging, maximum top node temperatures were raised to 52°C and 57°C and heat pump source temperatures were raised to 53°C and 58°C for DHW and SH, respectively. DHW was prioritized over SH and simultaneous charging of both tanks was not allowed. Opportunistic renewable charging status was determined using a PV threshold of 4 kW and wind threshold of 50 kW. The 4 kW PV threshold was used because the heat pump is non-modulable and forced charging is only desirable when most of the electricity is freely derived from PV. A net wind threshold of 50 kW was used because previous studies of the data indicate net generation above that threshold is more consistent and likely to endure, meaning the heat pump does not have to be turned on and off as frequently.

The *main.py* script was responsible for simulation. Once executed, *main.py* read in input data, specified initial simulation timestep and simulation length, and created year-long arrays of control temperatures, WSHP COP, opportunistic charging status, and prices. *main.py* then ran an iterative loop across the specified simulation period. In each loop, month and day of year counters were incremented and control values were reset. Tank temperatures were then calculated after meeting discharge demands during the timestep. After discharging was accounted for, an instance of the appropriate control class was initialized and used to calculate the node temperatures and charging status of each tank. Finally, *main.py* stored these temperatures with other metrics and exported them to three CSV files following the conclusion of the simulation loop.

4.3 Controls

This subsection describes the three control approaches used during simulation of the Woodside heating system. The controls were (1) demand-led RBC reflecting controls currently in place at Woodside; (2) opportunistic PV RBC that opportunistically charged tanks when PV generation exceeded a threshold; and (3) advanced RBC with opportunistic PV and wind charging and other control improvements. Efforts were made to adapt the MPC module in PyLESA for the purposes of this analysis, but they were unsuccessful and halted due to time limitations. These controls are described in greater detail below with an overview of general characteristics provided in Table 6.

Table 6. Overview of general control characteristics for the four control schemes implemented during simulations.

	Demand-Led RBC	*Opportunistic PV RBC*	*Advanced RBC*
Forced PV Charge	No	Yes	Yes
Forced Wind Charge	No	No	Yes
Night Offset	No	No	Yes
SH Shutdown	No	No	Yes

4.3.1 Demand-Led RBC

The demand-led RBC reflected current Woodside thermal storage and heat pump controls to the best knowledge of the author. This control was entirely demand-led; the tanks discharged to meet demand and charged immediately when node temperatures dropped below the charging threshold. There was no forced charging using renewables or adjustment of tank setpoint temperatures.

4.3.2 Opportunistic PV RBC

The opportunistic PV RBC implemented opportunistic PV charging. Opportunistic charging was triggered when (1) there was a PV surplus exceeding the 4 kW threshold and (2) the top node temperature did not exceed a limit of 50°C or 55°C for DHW or SH, respectively. During opportunistic charging, maximum top node temperatures were increased to 52°C and 57°C and heat pump source temperatures were increased to 53°C and 58°C for DHW and SH, respectively. The heightened storage temperature accelerated ambient losses, and greater heat pump output temperature decreased COP; however, it was expected that the benefit of cheaply storing energy using renewables outweighed these drawbacks.

4.3.3 Advanced RBC

The advanced RBC implemented forced PV and added forced wind charging, a nighttime offset in minimum node temperatures, and seasonal shutdown of the SH system. These features were proposed in pseudocode drafted by Paddy Atkinson as part of the POCIT project and adapted for this thesis. The other proposed features of a weather compensation curve for SH flow temperatures and smart DHW disinfection cycle charging were not implemented, as thermostatic mixing valves and the disinfection cycle were excluded from the analysis. Two control scenarios with advanced RBC were simulated, one with seasonal shutdown of the SH system and the other without, to determine the cost savings enabled by the shutdown.

Opportunistic charging was triggered when (1) there was a PV surplus exceeding the 4 kW threshold or wind surplus exceeding the 50 kW threshold and (2) the top node temperature did not exceed a limit of 50°C or 55°C for DHW or SH, respectively. During opportunistic charging, maximum top node temperatures were increased to 52°C and 57°C and heat pump source temperatures were increased to 53°C and 58°C for DHW and SH, respectively. As with the opportunistic PV RBC script, it was anticipated that the benefit of cheaply storing energy via renewable electricity would outweigh the drawbacks increased losses and worsened COP.

The night offset reduced the minimum node temperature that triggered tank charging. The rationale for the offset was that overnight demand, particularly for DHW, is likely minimal. Therefore, there is little need to maintain multiple nodes' worth of reserve water above the flow temperature and sustain higher losses. Offset minimum DHW and SH setpoints were set to 43°C and 45°C, respectively, for timesteps ranging from 19:00 to 9:00 each day.

The SH shutdown stopped the heat pump from charging the SH tank regardless of node temperatures during the summer months and select days of the shoulder season. The rationale for the shutdown was the lack of SH discharge in the Emoncms dataset between timesteps 7694 and 12400, approximately early June to mid-September. Repeatedly charging the tank and dissipating all the energy as heat loss would be inefficient. SH was disabled during June, July, and August, and enabled from October to April. During May, a counter tracked the number of days that experienced average ambient temperatures above 14°C. SH was disabled once the counter reached 6 days. During September, a counter tracked the number of days that experienced average ambient temperatures below 16°C. SH was enabled once the counter reached 6 days.

4.4 Tariffs

This subsection describes the tariff structures used while simulating the Woodside heating system. The tariffs were a simple flat-rate tariff currently offered to Findhorn residents; a day-night time-of-use tariff currently offered to Findhorn residents; and a selection of hypothetical dynamic wind-based tariffs. Table 7 provides an overview of these tariff structures.

4.4.1 Simple Tariff

The simple electricity tariff assumed PV electricity was free to Woodside and assigned a flat rate of £0.3407/kWh for all other consumed electricity. This was based on the flat rate option available at the park [2].

4.4.1 Day-Night Tariff

The day-night time-of-use tariff assumed PV electricity was free to Woodside and assigned variable rates for different times of day. Between 7:00 and 12:00, the rate was £0.3607/kWh. At all other times the rate was £0.3171/kWh. These were based on the time-of-use rate option available at the park [2].

Table 7. Overview of rates for PV, wind, and grid electricity under each tariff structure.

	Simple Tariff	*Day-Night Tariff*	*Dynamic Wind Tariff 1*	*Dynamic Wind Tariff 2*	*Dynamic Wind Tariff 3*
PV Rate (£/kWh)	0	0	0	0	0
Wind Rate (£/kWh)	0.3407	0.3607 morning / 0.3171 rest of day	0.18	0.15	0.12
Grid Rate (£/kWh)	0.3407	0.3607 morning / 0.3171 rest of day	0.45	0.45	0.475

4.4.2 Dynamic Wind Tariff

Three different dynamic wind tariffs (DWT) were assessed to probe the sensitivity of outcomes to specific wind and grid rates. This reflected uncertainty in the way a dynamic wind tariff may be implemented at Findhorn and for electrified heating systems in general. It was assumed that PV electricity was free to Woodside. Non-PV electricity rates changed dynamically depending on whether Findhorn was importing or exporting electricity. This was akin to the Agile pricing strategy introduced by Octopus Energy [43] that raises prices at peak demand periods and lowers prices when demand is low. In DWT 1, surplus wind electricity was priced at £0.18/kWh in line with FWP's estimated valuation [9]. Imported grid electricity was priced at £0.45/kWh to approximately average to the current standard rate of £0.3407/kWh over the year. In DWT 2, the wind rate dropped to £0.15/kWh, representing a situation in which NFD more actively incentivizes wind use. In DWT 3, the wind rate was lowered to £0.12/kWh and the import rate was raised to £0.475/kWh.

5.0 Simulation Result Analysis

This section describes the results and KPIs obtained from simulations of the Woodside heating system. OCOH, annual total cost, renewables utilisation, and carbon intensity are compared for each combination of controls and tariffs. Then, a graphical analysis of node temperatures and renewable generation is conducted for each control regime over a windy period, a sunny period, and a period with low renewables generation.

5.1 Quantitative Result Analysis

This subsection details the KPIs for the simulated control and tariff scenarios. The OCOH, gross annual heating cost, renewables utilisation, and carbon intensity are presented in Table 8. These metrics are briefly discussed and compared across simulated scenarios.

Table 8. KPIs for the four simulated controls with each of the five simulated tariffs.

Control	*Tariff*	*OCOH ($£/kWh_{th}$)*	*Annual Cost (£)*	*Renewables Utilisation (%)*	*Carbon Intensity (gCO_2eq / kWh_{th})*
Demand-Led RBC	*Standard*	0.1458	2161	37.0	81.2
	Day-night	0.1422	2108	37.0	81.2
	DWT 1	0.1593	2361	37.0	81.2
	DWT 2	0.1556	2306	37.0	81.2
	DWT 3	0.1595	2364	37.0	81.2
Opportunistic PV RBC	*Standard*	0.1365	2023	41.3	78.1
	Day-night	0.1335	1978	41.3	78.1
	DWT 1	0.1496	2218	41.3	78.1
	DWT 2	0.1462	2167	41.3	78.1
	DWT 3	0.1500	2223	41.3	78.1
Advanced RBC (SH seasonally disabled)	*Standard*	0.1344	1992	51.2	63.8
	Day-night	0.1326	1966	51.2	63.8
	DWT 1	0.1332	1974	51.2	63.8
	DWT 2	0.1283	1901	51.2	63.8
	DWT 3	0.1291	1913	51.2	63.8

Advanced RBC (SH not seasonally disabled)	*Standard*	0.1350	2001	52.5	64.2
	Day-night	0.1333	1976	52.5	64.2
	DWT 1	0.1335	1978	52.5	64.2
	DWT 2	0.1285	1905	52.5	64.2
	DWT 3	0.1293	1916	52.5	64.2

5.1.1 Renewables Utilisation

Renewables utilisation did not vary as the tariff changed because the opportunistic controls did not explicitly consider the price of electricity. Instead, operation was controlled based on renewables availability. As the controls became more complex, renewables utilisation increased substantially. The demand-led RBC utilisation of 37.0% increased to 41.3% when opportunistic charging with PV was implemented, an absolute increase of 4.3% and relative increase of 11.6%. Advanced RBC's introduction of opportunistic wind charging further increased renewables utilisation to 51.2%, an absolute increase of 14.2% and relative increase of 38.4% compared to the demand-led RBC. This indicated that advanced RBC could substantially increase renewables utilisation for thermal store charging. Raising the heat pump charging temperatures during opportunistic charging may enable increased renewables utilization. This is because the tank can "coast" at a higher temperature for longer before forced charging, increasing the likelihood that an opportunistic charging period will present itself.

Renewables utilisation was marginally higher for advanced RBC when SH was not seasonally disabled. This can be explained by increased total electrical use in the summer, when PV was abundant and frequently output more than the 4 kW charging threshold. When SH was not seasonally disabled, total PV consumption increased 14.4% relatively and 166 kWh in total, while wind use increased by only 1.1% or 28 kWh and grid use decreased marginally by 2 kWh (Table 12, Appendix 2). This boosted renewables utilisation but marginally increased OCOH because the end-use heat provided to Woodside residents remained constant while the increase in wind consumption had to be paid for.

5.1.2 Carbon Intensity

Carbon intensity was correlated to renewables utilisation and varied between control regimes. However, changes in tariffs had no impact on carbon intensity. Decreasing carbon intensity was correlated with increased control complexity and opportunistic charging. The baseline intensity of 81.2 gCO_2eq/kWh_{th} decreased 3.8% to 78.1 gCO_2eq/kWh_{th} under the opportunistic PV RBC; this was less than the 11.6% relative increase in renewables utilisation. Using advanced RBC, carbon intensity dropped further to 63.8 gCO_2eq/kWh_{th}, a 21.4% decrease compared to the demand-led RBC. Again, this was less than the 38.4% increase in renewables. These results suggest that increased renewables utilisation via opportunistic charging is an effective way to lower heating carbon intensity. However, the relationship between increased renewables share and decreased carbon intensity was not direct; this may be attributable to different carbon intensities of wind and PV constituting the whole renewable supply.

5.1.3 OCOH and Gross Cost

The lowest simulated OCOH was £0.1283/kWh_{th} using advanced RBC with DWT 2, and the highest was £0.1595/kWh_{th} using demand-led RBC with the DWT 3. A more realistic comparison was between demand-led RBC with the standard tariff and advanced RBC with DWT 2. These scenarios had OCOH of £0.1458/kWh_{th} and £0.1283/kWh_{th}, indicating a 12.0% cost reduction that brought gross annual costs from £2161 to £1905 for expected savings of ~£250 annually.

Further comparison of the scenario results revealed cost trends. Holding the tariff constant, increased control complexity generally reduced OCOH and gross costs over the simulation period. This could be attributed to increased renewables utilisation as discussed in Section 5.1.1 and the lower (or equivalent) costs of PV and wind relative to grid imports. An exception was that disabling SH over the summer produced a marginal OCOH decrease of less than a thousandth of a pound per kWh compared to the simulation without disabled SH. This could be explained by the underlying charging figures. Although annual electricity use was reduced by 192 kWh or 2.7%, 86% of this reduction canes from reduced PV usage (Appendix 2, Table 2). There was no appreciable cost saving because PV is free to Woodside.

Varying the tariffs produced different results depending on the control regime. Across controls, the day-night tariff reduced OCOH between 1% and 2.5%. This could be due to an increased frequency of charging outside the high-cost early morning period caused by residents depleting the DHW tank with after-work demand. The dynamic wind tariffs increased cost relative to the standard and day-night tariff for the demand-led and opportunistic PV RBC, but lowered costs for the advanced RBC. This was because the demand-led and opportunistic PV RBC do not opportunistically charge during wind surpluses. As a result, simulations with those controls had significantly lower wind consumption and greater grid imports compared to the advanced RBC scenarios (Appendix 2, Table 12). Heightened import prices therefore outweigh cheaper wind electricity under demand-led and opportunistic PV RBC. Because the advanced RBC enabled opportunistic wind charging, it captured the benefit of lower wind prices through significantly increased renewables utilisation.

Dynamic wind tariffs results are only discussed using advanced RBC because they do not provide a benefit for the other controls. In general, DWTs did not substantially alter OCOH compared to the existing Findhorn tariff options. DWT 1, 2, and 3 all resulted in an OCOH below the standard tariff £0.1344/kWh_{th}, but the greatest reduction to £0.1283/kWh_{th} using DWT 2 was only a 4.6% decrease. This decrease corresponded to annual gross savings below £100. Simulating with DWT 1 decreased the price of wind electricity by 16% from £0.18/kWh to £0.15/kWh but reduced OCOH by only 3.7% (Table 8). DWT 3 reduced wind cost further while increasing import costs correspondingly but marginally increased OCOH compared to DWT 2, which can be explained by the system using more imported than wind electricity over the year (Appendix 2, Table 12). Overall, this analysis indicated thhe examined dynamic wind tariffs lowered electricity costs compared to the existing tariffs, but only marginally. Greater cost reductions may require either lower wind pricing or alterations to the control regime.

5.1.4 Additional Results and Results Feasibility

Additional results of interest for each scenario are provided in Appendix 2. These include annual totals for electricity used to charge the SH and DHW tanks; thermal charge to the SH and DHW tanks; electricity usage from PV, wind, and grid imports; total carbon emissions; and thermal discharge from SH and DHW, which is the same for all scenarios.

The simulated node temperatures were reviewed to ensure that infeasible results did not occur. The foci of this review were minimum top node temperature, minimum temperature of any node, and the maximum temperature of any node. Minimum tank temperature should not fall below the return temperature, while maximum tank temperature should not exceed charging water temperature from the WSHP. The minimum top node temperature should ideally never go below the required flow temperature but may occasionally do so within the SH tank when the WSHP has prioritized DHW tank charging. No infeasible minimum or maximum temperatures were observed in any scenario, while the SH tank top node temperature only dropped below the 45°C flow temperatures for a handful of timesteps in each scenario.

5.2 Graphical Result Analysis

This subsection contains a graphical analysis of system behavior during simulation. The analysis focused on node temperatures, charging events, and renewable generation over three-day periods for each control regime. Tariffs were not considered because the controls triggered charging based on renewables availability, not cost. The first period was between timesteps 12000 and 12143, corresponding to the dates September 7 to 9, which had significant solar generation. The second period was between timesteps 624 and 767, corresponding to the dates January 14 to 16, which had significant wind generation. A solar-driven period outside of the summer months was selected to show advanced RBC SH charging behavior.

5.2.1 Demand-Led RBC

This subsection analyzes system operation under demand-led RBC.

5.2.1.1 *High PV Generation*

The behavior of the system during the high-PV period is shown in Figure 9. Wind generation is excluded because its greater magnitude makes the PV generation difficult to see. Rapid charge/discharge cycles were observed for the DHW tank. SH cycles were less frequent and primarily triggered by losses, as SH demand was low at the tail end of summer. Temperatures remained within the desired boundaries, indicating the models functioned as expected.

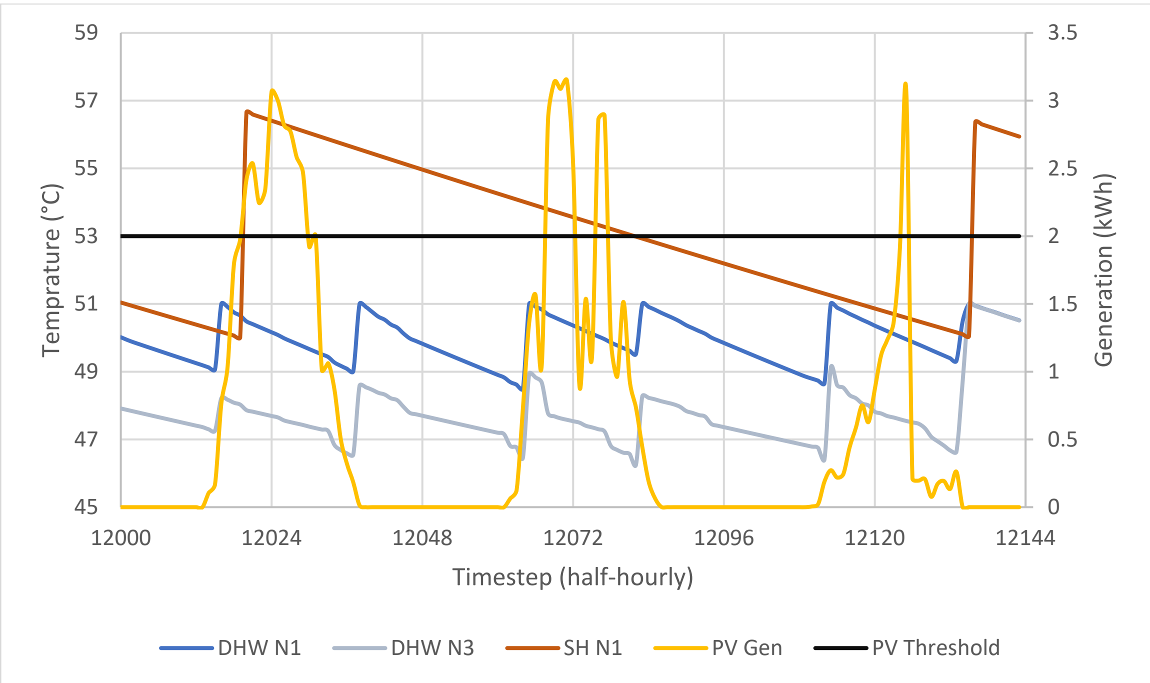

Figure 9. Simulated system behavior under demand-led RBC during the high-PV generation period.

PV's cyclical generation profile is seen with generation peaking midday. Generation exceeded the specified charging threshold of 4 kW, or 2 kWh per half-hour timestep, on each day during this period. Although charging cycles may have incidentally overlapped with PV generation, the clear lack of coordination between renewables availability and tank charging is evident. Consider the PV peak on the third day, which occurred merely hours before the SH and DHW tanks both charge. This reflects that demand-led RBC left significant room for increased use of onsite renewables, corroborating the findings of the quantitative analysis.

5.2.1.2 *High Wind Generation*

The simulated heating system behavior during the high-wind period is shown in Figure 10. PV generation is excluded, as changes in output are difficult to see due to scaling. In this winter period, SH and DHW both cycled frequently due to high heat demands. Tank temperatures remained within the desired boundaries.

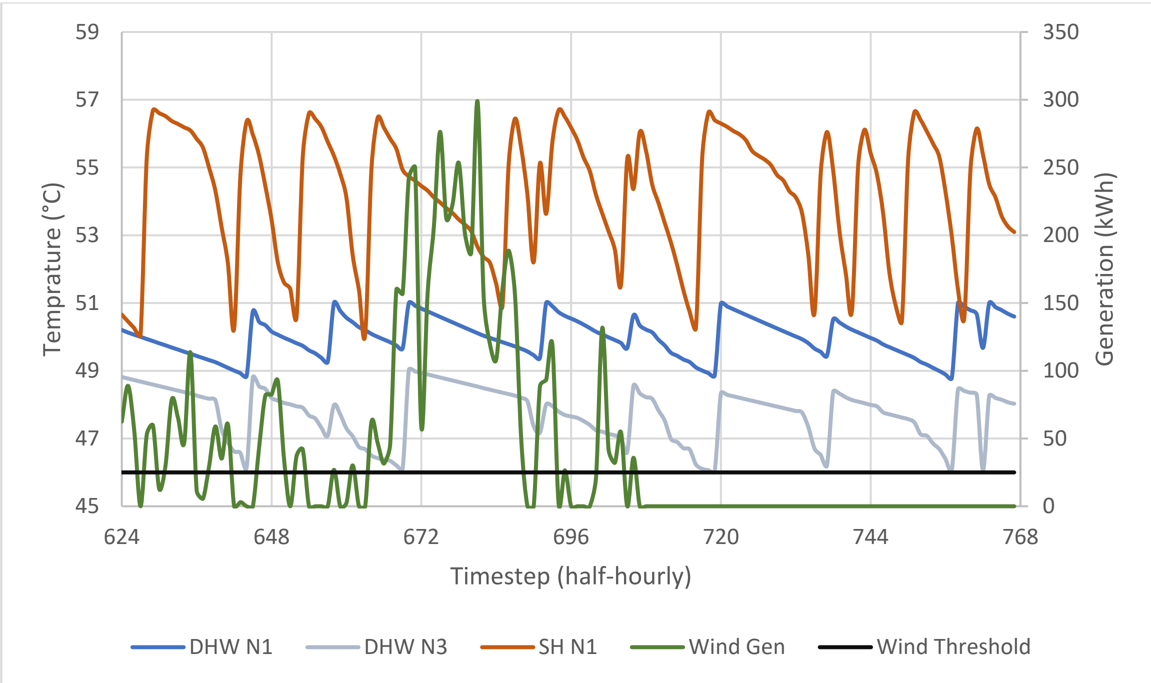

Figure 10. Simulated system behavior under demand-led RBC during the high-wind generation period.

Wind had a less regular profile than PV, though its magnitude was greater. Wind generation exceeded the specified charging threshold at several points throughout the first half of this period. This incidentally led to significant use of wind for charging. The lack of opportunistic charging with demand-led RBC was observed during the period of the highest wind generation between timesteps 672 and 684, when neither the DHW nor SH tank charged. This again shows that the demand-led RBC failed to capture available renewables utilisation gains.

5.2.2 *Opportunistic PV RBC*

This subsection analyzes system operation under opportunistic PV RBC.

5.2.2.1 High PV Generation

System behavior during the high-PV period is shown in Figure 11. The cyclical generation profile of PV, prioritization of DHW charging, and variation of top node temperatures within the expected boundaries indicated the tank models are functioning properly.

As this control regime utilizes opportunistic PV charging, several changes to system operation are observable between Figures 9 and 11. PV generation and charging were now much better aligned; all SH charging cycles and two out of three DHW charging cycles were triggered by PV. SH charging cycles were more frequent because the threshold temperature to allow opportunistic charging exceeded the threshold temperature for forced charging. DHW tank cycling was less frequent because the opportunistic charging heated the tank to a higher temperature. This allowed the tank to coast longer in wait of the next opportunity for PV charging before it was forced to charge due to low node temperatures.

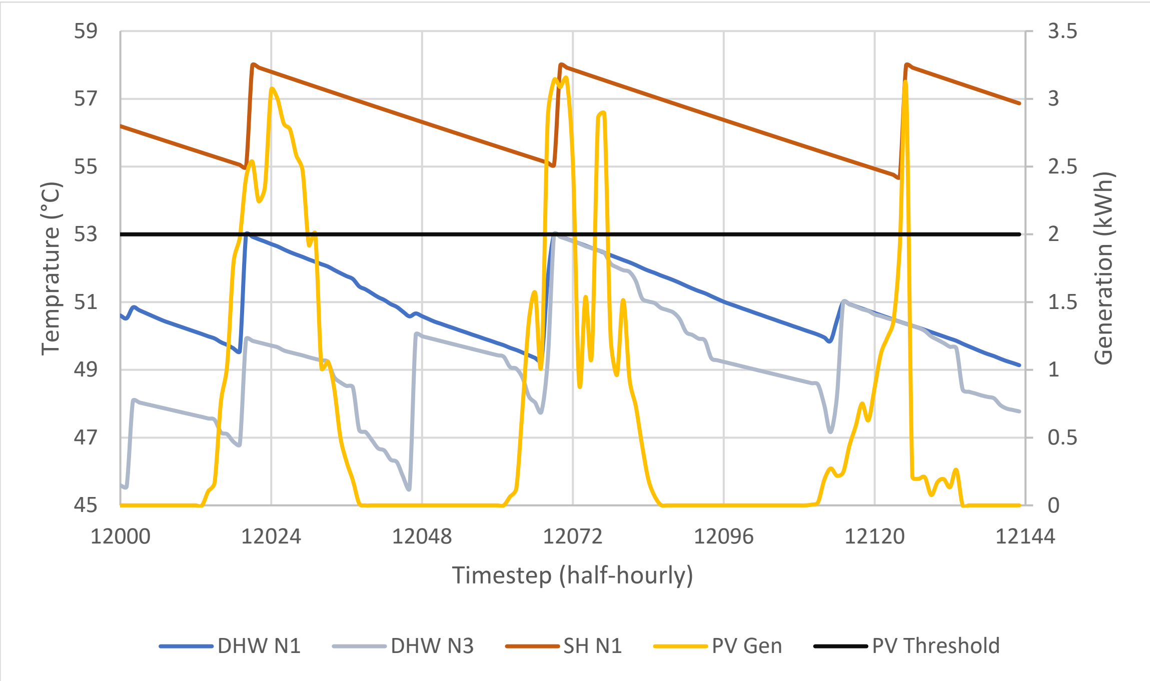

Figure 11. Simulated system behavior under opportunistic PV RBC during the high-PV generation period.

However, Figure 11 indicates there was still scope for increased renewable use. Extrapolating the DHW tope node temperature to the third PV generation peak suggests the DHW temperature would not drop below the flow temperature before being able to charge using PV instead of imported electricity. Therefore, a capability to temporarily lower forced charging temperature setpoints in anticipation of the daily PV cycle would improve the opportunistic PV RBC. This aligns with the findings of the quantitative analysis that show the advanced RBC achieved cheaper OCOH with the use of a night offset.

5.2.2.2 High Wind Generation

System behavior during the high-wind period is shown in Figure 12. Maintenance of node temperatures within the expected boundaries indicated proper model function.

Because the opportunistic PV RBC did not opportunistically charge using wind, Figure 12 is essentially identical to Figure 10. The same conclusions can be drawn, namely that opportunistic PV RBC missed a substantial opportunity for opportunistic wind charging. Opportunistically charging to a heightened temperature would make better direct use of wind and allow the tanks to coast longer, increasing the likelihood they can charge renewably before being forced to charge with imports. This aligned with the KPIs showing that advanced RBC achieves lower LCOH by increasing renewables utilisation with opportunistic wind charging.

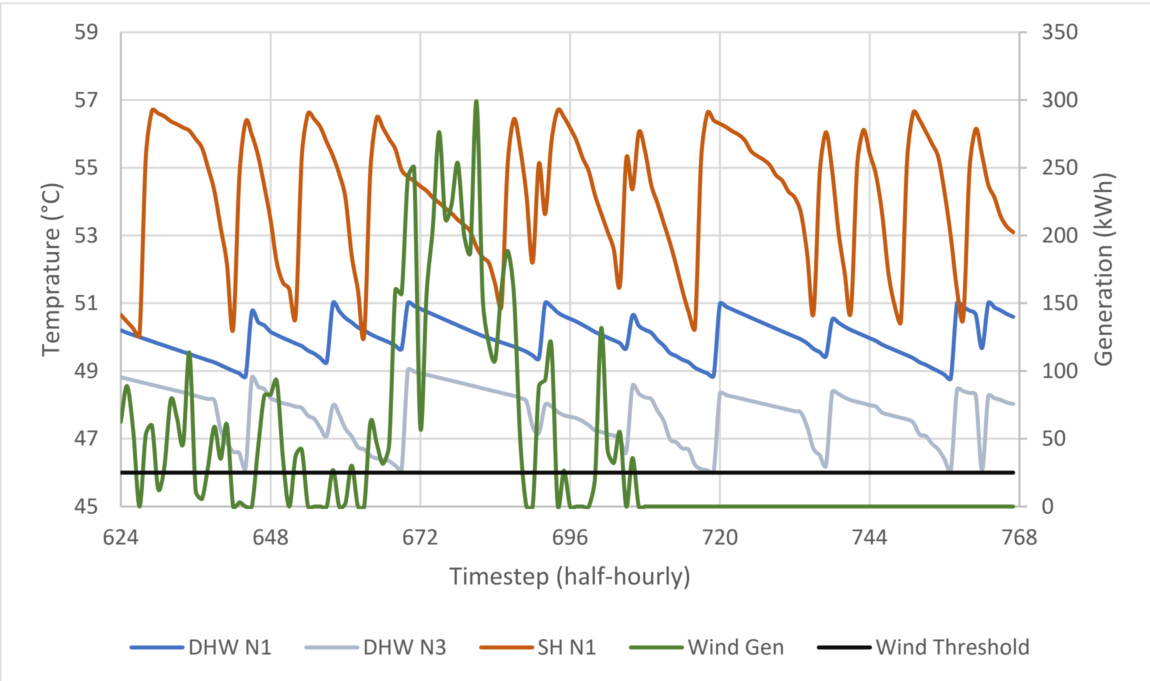

Figure 12. Simulated system behavior under opportunistic PV RBC during the high-wind generation period.

5.2.3 Advanced RBC with Seasonally Disabled SH

This subsection analyzes system operation under advanced RBC with seasonally disabled SH. Advanced RBC without seasonally disabled SH will have substantively identical behavior, except that SH charging will not occur in the summer.

5.2.3.1 High PV Generation

System behavior during the high-PV period is shown in Figure 13. The cyclical generation profile of PV, prioritization of DHW charging, and variation of top node temperatures within the expected boundaries indicate the tank models were functioning properly.

Although advanced RBC and opportunistic PV RBC both opportunistically use PV, Figures 11 and 13 show clear differences. Notably, PV was not used to opportunistically charge the DHW tank for the first two observed charge cycles. This was because the minimum temperature in the third node dropped below the lower threshold before PV became available, and the top node temperature was then above the limit temperature for opportunistic charging. A potential solution is to increase the top node limit temperature above which opportunistic charging is not allowed; another is to directly control DHW forced charging using the top node temperature.

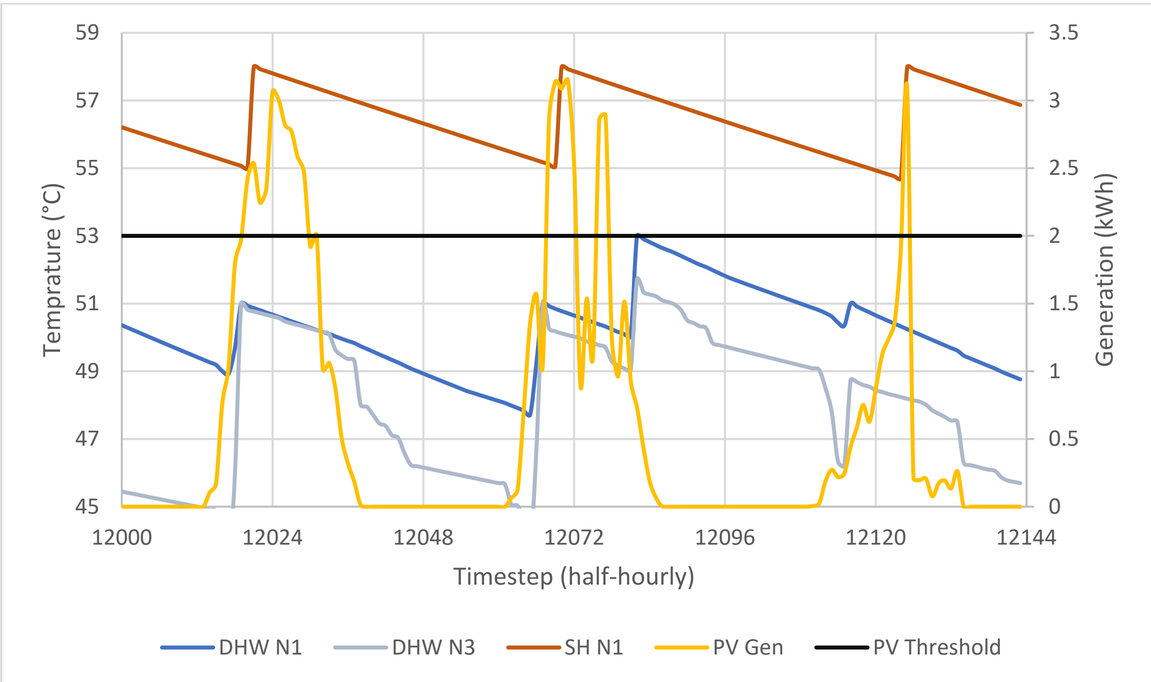

Figure 13. Simulated system behavior under advanced RBC during the high-PV generation period.

A period of opportunistic DHW charging did occur around timestep 12084, but PV generation was below the threshold at that time, so charging was presumably driven by wind. This behavior is suboptimal because free PV was abundant only a few hours before the opportunistic wind charge, and wind has an associated cost even if a dynamic wind tariff is considered. This highlights why a predictive controller may improve upon advanced RBC.

5.2.3.2 High Wind Generation

System behavior during the high-wind period is shown in Figure 14. Maintenance of node temperatures within the expected boundaries indicated proper model function.

With the introduction of opportunistic wind charging, the system behavior changed significantly. Opportunistic charging of the DHW and SH tanks brought them to heightened node temperatures and allowed them to coast until the next period of sufficient surplus wind during the first half of the examined period. This demonstrated why advanced RBC achieves higher renewables utilisation and lower OCOH than demand-led or opportunistic PV RBC. During the second half of the period, wind generation fell off and the tanks started to charge using imports. However, this charging was deferred because of the heightened starting temperatures and the night offset, as was shown by the SH top node temperature dropping to 45°C before charging was triggered. Over the year, this coasting prevented unnecessary charging and increases renewable use. It also reduced the number of total cycles, potentially reducing wear on the WSHP.

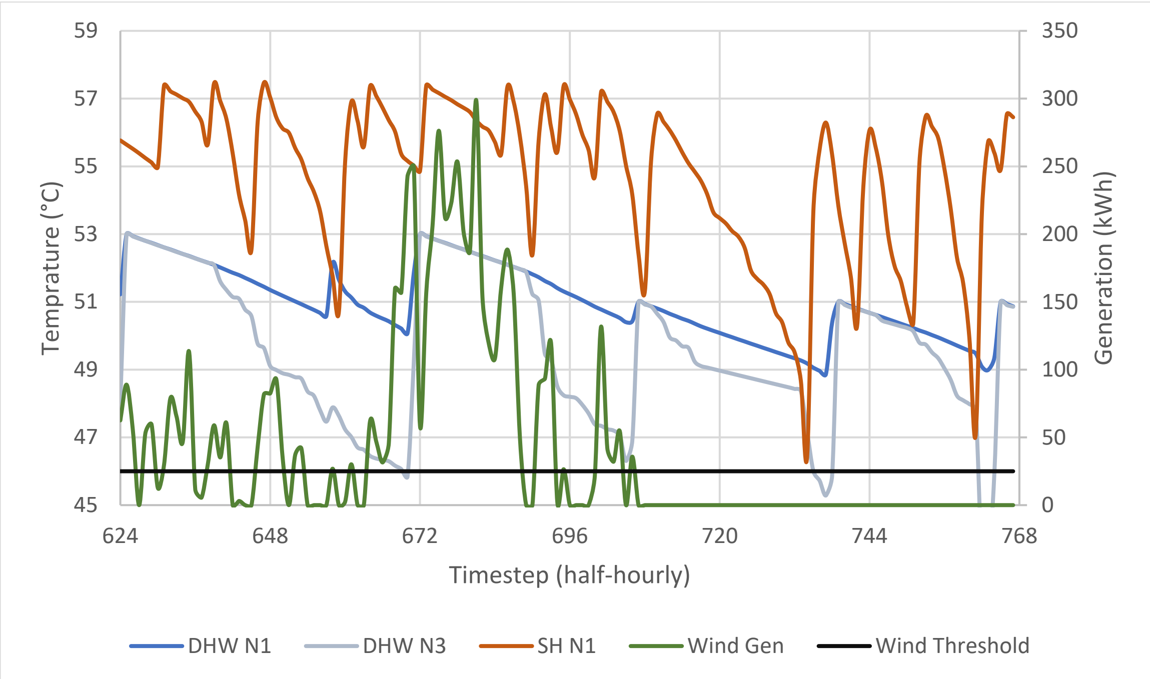

Figure 14. Simulated system behavior under advanced RBC during the high-wind generation period.

5.3 Key Takeaways

The simulated scenarios demonstrated that advanced RBC can achieve moderate reductions in heating costs for district heating systems with thermal storage. A 12.0% reduction in OCOH, from £0.1458/kWh_{th} to £0.1283/kWh_{th}, was expected when switching from demand-led RBC with the standard tariff to advanced RBC with DWT 2. However, the scale of the Woodside system meant that gross cost savings (on the order of ~£250 annually) were minimal. On the other hand, renewables utilisation increased by a substantial 38.4% and carbon intensity fell by 21.4% when switching to advanced RBC. Findhorn must assess whether the limited cost savings, but noticeable emissions reductions, warrant the time and effort required to implement these controls. This analysis found that tariffs have a less significant impact on costs. A graphical analysis gave further insight into why opportunistic charging was effective at both increasing renewables utilisation and lowering costs. By charging to high temperatures using free PV and cheap wind, the tanks could then coast for long periods of time before forced charging was required.

6.0 Discussion

This section presents key achievements, limitations of the current work, and avenues for future work to build upon these achievements and address the limitations.

6.1 Key Findings / Achievements

The work presented in this thesis addresses the three overarching aims specified in Section 1.3.

The first-principles multi-node PyLESA tank models inherited from Graeme Flett were documented and modified to represent the Woodside SH and DHW tanks. Empirical heat loss parameters were used and calibrated against periods of monitored data without charging or discharging. Finally, tank node masses were adjusted during a validation process until the tank model behavior resembled monitored outputs over a two-week period. These models were made available in a GitHub repository.

Python control scripts for a demand-led RBC, opportunistic PV RBC, and advanced RBC were written; an attempt was also made to adapt the MPC module in PyLESA. Existing tariff structures at Findhorn were identified and three potential implementations of a dynamic wind tariff were formulated. Data was obtained from the Emoncms portal for part of 2023 and 2024 and processed to produce complete annual datasets of Woodside SH and DHW demand, Findhorn electrical demands, and wind and PV generation. The control scripts, tariffs, data, and tank models were then applied to simulate Woodside heating system behavior over a year in half-hour timesteps under each combination of control regime and tariff. The control scripts and datasets were made available with the tank models.

Finally, the results of the simulations were compared to identify which combination of controls and tariffs produced the best KPIs. Quantitative analysis identified a potential cost reduction of 12.0%, corresponding to ~£250 annually, by switching from the current demand-RBC with a standard tariff at an OCOH of £0.1458/kWh$_{th}$ to advanced RBC with DWT 2 at an OCOH of £0.1283/kWh$_{th}$. Simulations indicated this switch also increased renewables utilisation from 37.0% to 51.2% and reduced carbon intensity by 21.4%. A graphical analysis was conducted to elucidate the mechanisms by which opportunistic control achieved these gains. These mechanisms are improved alignment of charging with generation and tank coasting enabled by raised charging temperatures during opportunistic charging.

6.2 Limitations

The achievements of this thesis come with several limitations.

6.2.1 Woodside System Modelling

Although the multi-node tank models were more accurate than simple energetic or moving boundary models, they did not perfectly mimic observed behavior. This could partly be attributed to simplifying assumptions. Both models assumed that the tank is a perfect cylinder. The DHW tank model used heat loss coefficients that were not physics-based, but were calibrated to align with observed heat loss. For the SH tank model, it was assumed that conductive heat loss only occured linearly, that insulation provided the only resistance to heat flow, and that the heat loss from piping connections was spread evenly across the nodes. Despite these limitations, model calibration and validation indicated the tank models approximated measured performance reasonably well.

A limitation of the model is that heat pump COP was calculated assuming an average monthly source water temperature. In reality, temperatures fluctuate significantly across the month and across each day. Real water temperatures may drop below the 5°C minimum heat pump inlet temperature during the winter, necessitating direct electric preheating up to 5°C. The model did not account for this temperature fluctuation or water preheating.

During simulation, non-heat electrical demand at the site was not considered as a potential competitor for the use of onsite renewable generation. This primarily affected PV generation, as opportunistic wind charging occured only when the net Findhorn electricity surplus exceeded 50 kW, which was far greater than the 4 to 7 kW drawn for the Ochsner WSHP at Woodside. A potential consequence is that the simulated gains of opportunistic charging were overstated because some of the PV used to charge the thermal stores was already used to meet electrical demand. This could increase domestic electrical costs for Woodside residents, eating into the expected heating cost reduction of advanced RBC.

Finally, this analysis is limited to controlling existing thermal storage assets at Woodside. There is no consideration of the potential for additional storage, either in the form of water tanks or phase change materials.

6.2.2 Site Data

The limitations regarding site data are primarily related to missing 2023 data, how well the data reflect future site conditions, and methods used to calculate Woodside heating demands. The hybrid 2023 datasets for the West Whins, CB001, and CB002 feeds may not accurately reflect site conditions. This uncertainty is considerable for West Whins considering three-quarters of the hybrid 2023 dataset is pulled from 2024 or replicated from other parts of the year.

An additional limitation is that wind generation in future years is likely to vary from that in the 2023 dataset. This is due to aging turbines [75], inter-year weather variability [76], and broader changes in climate [77]. To a limited extent, these factors also impact PV generation. Therefore, extrapolating the benefits of opportunistic charging estimated in this thesis to future years may result in an overestimation or underestimation.

Furthermore, site data describing outlet temperatures and return temperatures for the water tanks over the year could not be accessed. This was likely because the feeds were not operating properly or the data was monitored but not logged. As a result, Woodside heating demands at half-hourly timesteps were estimated based on volumetric flow out of the tanks and assumed temperatures. These temperatures are unlikely to be constant over the year, introducing error in the calculation of OCOH because the actual heat provided to properties during 2023 is uncertain. Beyond the simplified calculation, determining the cost of heat provided for DHW is a challenge because it is unknown how the end user uses the hot water. This work assumes that the heat used is a function of the flow temperature and temperature of water returning to the DHW tank through the Living Machine wastewater system. However, future studies may prefer to measure the annual cost of DHW in volumetric terms.

6.2.3 Controls and Tariffs

The primary limitation associated with controls was that simulations were not conducted with a predictive controller. Attempts were made to use the MPC module in PyLESA, but were abandoned due to a lack of success and time limitations. As the graphical analysis of the advanced RBC indicates, there was additional scope for increased renewables utilisation beyond opportunistic controls that is not assessed in this work.

The controls implemented in this work did not operate DHW disinfection cycles, which are meant to occur at least every 10 days to prevent Legionella growth [78]. Running disinfection cycles would increase electricity demand without increasing the heat provided to end users, raising OCOH across control and tariff scenarios. The controls also did not implement a weather compensation curve for the SH tank proposed as part of the POCIT project. A compensation curve would lower flow temperatures below 45°C in response to warmer ambient temperatures. This would likely lower costs, as the SH tank would not have to be charged to such a high temperature and WSHP COP would increase due to the lower temperature differential.

The tariffs assumed to be in place at Findhorn were based on the information available on the NFD website [2]. These tariffs may fluctuate in the future, impacting the validity of extrapolating simulation results to future years. The formulated dynamic wind tariffs represent a few possible rates, but tariff design is an active area of innovation with a multitude of other options [79]. This analysis has only scratched the surface of all the tariffs that could be implemented at Findhorn.

Finally, this analysis does not consider how costs (and savings from opportunistic control) associated with tank charging might be distributed among Woodside residents. Cost distribution is a challenge because the costs of charging the tanks are temporally dissociated with the use of heat from the tanks, and much of the heat is lost to the environment. This concern is unlikely to impact the benefit of controls because end-user demand is not impacted in any way. However, it is an important consideration for communal energy schemes that target load shifting, especially regarding how motivated residents are to adopt advanced controls.

6.3 Recommendations for Future Work

Several areas of future work could build upon the achievements of this thesis and address the associated limitations. Recommendations considered to be most pertinent are presented here.

6.3.1 Improving and Expanding Simulation of Woodside

A straightforward extension of this work is simulating system performance with adjusted control settings. The first steps would be exploring how costs change when extending the night offset into the day and lowering the wind generation threshold for opportunistic charging. A lengthened night offset would extend the coasting period, potentially affording an increased opportunity for PV charging during the day. Similarly, lowering the wind threshold below 50 kW could increase the frequency of wind charging, but may decrease the occurrence of opportunistic PV charging. Simulating with higher WSHP flow temperatures during opportunistic charging could elucidate the optimal balance between COP, renewables utilisation, and subsequent heat losses. Raising the DHW and SH tank limit temperatures, which are the thresholds above which opportunistic charging will not occur, may also enable increased opportunistic charging and warrants investigation. Finally, simulating with increased temporal resolution – such as 15-minute timesteps – may offer additional system insights.

Instead of adjusting control parameters, future work could also examine alternative tariff options. There is broad scope to explore different settings for the examined time-of-use and dynamic tariff types as well as additional tariffs tied to wholesale markets such as Octopus Agile [43]. These rate designs may synergize with MPC, which is another area of future work that could reduce costs and increase renewables utilisation. Other studies [80], [81] indicate that MPC provides significant benefits in related domains like building energy management, so it is worthwhile to investigate its application to the Woodside heating system.

An alternative direction for future work is improving the water tank models. Developing heat loss parameters for the SH tank could increase model accuracy if node temperature readings could be obtained at intermediate points along the tank. Implementing more complex model types such as a zonal model or CFD may clarify the trade-off between accuracy and computational burden while modelling the Woodside system.

The final set of suggestions for future work directly address the limitations of the current simulation approach. Obtaining more detailed water temperature data at hourly resolution could enable the model to account for WSHP inlet water preheating. Monitored flow and return temperature values for the SH and DHW tanks would enable significantly more detailed calculation of energy demands at Woodside, increasing the relevance of simulation results. Finally, implementing disinfection cycle charging would enable more realistic simulation of DHW tank behavior.

6.3.2 Broadened System Focus

Broadening the analysis and simulation focus to extract lessons that are applicable to heating systems beyond Woodside is another avenue for future work.

The Woodside WSHP can only operate at its maximum output, so whenever it opportunistically charges it will use grid electricity if renewable supply is insufficient. A future work would simulate system operation using a modulable heat pump. This type of heat pump can adjust its output to align exactly with the amount of available renewable electricity. Understanding whether modulable heat pumps offer benefits that warrant increased prices compared to non-modulable options is a valuable future work for communities considering district heating with thermal storage.

Comparing hot water tanks to alternative forms of thermal storage, such as phase change materials [82], is another possible direction. Pairing a detailed BEMS that can efficiently manage energy flows at the household level with this model of thermal storage may be fruitful in magnifying costs reductions through more efficient energy use and decreased heat demands. Additionally, "recursive" development could be pursued by integrating the multi-tank heating system approach into PyLESA, which natively models systems with a single hot water tank. PyLESA's range of applicability could also be expanded by integrating the indirectly charged DHW tank model developed in this thesis. In a future version of PyLESA, this model could be presented to the user as one of several options.

6.3.3 Real-World Implementation and Feedback

These simulations can be taken a step further by conducting a trial run of the advanced RBC at Woodside and observing how real system performance compares to predicted performance. This would require adjusting the controls code for compatibility with the Raspberry Pi used in monitoring and control and uploading the code to the Pis via Node-RED.

In the same vein, a tool incorporating this Woodside model could be developed that quickly predicts the effects of different tariff options on electricity and heating costs at Findhorn as a whole. Such a tool would benefit Findhorn when it engages in negotiation for import and export contracts, as the window to accept or decline is brief, and it is currently challenging to fully understand the benefits and drawbacks of different contract options. However, the development of such a tool would require significant additional development of models for other Findhorn neighborhood to provide any useful results.

7.0 Conclusion

This thesis work developed validated models for the Woodside DHW and SH water tanks and control scripts for demand-led RBC, opportunistic PV RBC, and advanced RBC. The model and scripts were used to simulate system behavior under a range of tariffs, finding an annual cost saving of 12.0% and carbon intensity reduction of 21.4% when advanced RBC is applied with the second dynamic wind tariff. Notable limitations include simplified calculation of site heating demand, the exclusion of DHW disinfection cycles from the model, and the lack of predictive controls. Opportunities for future work that build upon this thesis include additional simulations with varied temperature and control setpoints; simulation with a predictive controller; and analysis with a hypothetical modulable heat pump that can inform the design of future district heat and thermal storage systems. The tank models and control scripts have been shared at https://github.com/eli-d-strath/woodside_control and passed forward to PhD student Isaac Whitelaw for future site analysis.

8.0 References

[1] P. Atkinson, "Energy Masterplan for The Park Findhorn 2021." New Findhorn Directions Ltd, Jun. 2021. Accessed: Jul. 30, 2024. [Online]. Available: https://www.newfindhorndirections.co.uk/energy-masterplan/

[2] "Electricity Prices." Accessed: Jul. 30, 2024. [Online]. Available: https://www.newfindhorndirections.co.uk/electric/price/

[3] "Electric," New Findhorn Directions. Accessed: Jul. 30, 2024. [Online]. Available: https://www.newfindhorndirections.co.uk/electric/

[4] DigiRoutes, "Affordable Housing - Community Owned," Park EcoVillage Trust Findhorn, Moray, Scotland. Accessed: Jul. 30, 2024. [Online]. Available: https://parkecovillagetrust.co.uk/affordable-housing/

[5] DigiRoutes, "North Whins," Park EcoVillage Trust Findhorn, Moray, Scotland. Accessed: Jul. 30, 2024. [Online]. Available: https://parkecovillagetrust.co.uk/affordable-housing/north-whins-2/

[6] P. Atkinson, "M01 AS BUILT - Plant Room & Heat Network Schematic." Park Ecovillage Trust, May 26, 2023.

[7] "Akva EK 1500 accumulator." Accessed: Jul. 30, 2024. [Online]. Available: https://www.northmangroup.co.uk/Akva_EK_1500.html

[8] "Stainless Cylinders - McCallum Water Heating." Accessed: Jul. 30, 2024. [Online]. Available: https://www.mccallumwaterheating.co.uk/stainless-cylinders.php

[9] D. Easter, "Windfall Discounts | Findhorn Wind Park." Accessed: Aug. 05, 2024. [Online]. Available: https://findhornwind.co.uk/windfall-discounts/

[10] S. Nicholson and G. Heath, "Life Cycle Greenhouse Gas Emissions from Electricity Generation: Update." NREL, Sep. 2021.

[11] M. Ozoemena, W. M. Cheung, and R. Hasan, "Comparative LCA of technology improvement opportunities for a 1.5-MW wind turbine in the context of an onshore wind farm," *Clean Technol. Environ. Policy*, vol. 20, no. 1, pp. 173–190, Jan. 2018, doi: 10.1007/s10098-017-1466-2.

[12] "SSE plc Annual Report 2023." Scottish and Southern Energy plc, 2023. Accessed: Aug. 06, 2024. [Online]. Available: https://www.sse.com/media/pf3fsfak/sse-plc-annual-report.pdf

[13] M. Howells *et al.*, “OSeMOSYS: The Open Source Energy Modeling System: An introduction to its ethos, structure and development,” *Energy Policy*, vol. 39, no. 10, pp. 5850–5870, Oct. 2011, doi: 10.1016/j.enpol.2011.06.033.

[14] Md. K. Islam, J. M. Akanto, M. Zeyad, and S. M. M. Ahmed, “Optimization of Microgrid System for Community Electrification by using HOMER Pro,” in *2021 IEEE 9th Region 10 Humanitarian Technology Conference (R10-HTC)*, Sep. 2021, pp. 01–05. doi: 10.1109/R10-HTC53172.2021.9641615.

[15] J. Després, N. Hadjsaid, P. Criqui, and I. Noirot, “Modelling the impacts of variable renewable sources on the power sector: Reconsidering the typology of energy modelling tools,” *Energy*, vol. 80, pp. 486–495, Feb. 2015, doi: 10.1016/j.energy.2014.12.005.

[16] A. Lyden, R. Pepper, and P. G. Tuohy, “A modelling tool selection process for planning of community scale energy systems including storage and demand side management,” *Sustain. Cities Soc.*, vol. 39, pp. 674–688, May 2018, doi: 10.1016/j.scs.2018.02.003.

[17] H.-K. Ringkjøb, P. M. Haugan, and I. M. Solbrekke, “A review of modelling tools for energy and electricity systems with large shares of variable renewables,” *Renew. Sustain. Energy Rev.*, vol. 96, pp. 440–459, Nov. 2018, doi: 10.1016/j.rser.2018.08.002.

[18] C. Klemm and P. Vennemann, “Modeling and optimization of multi-energy systems in mixed-use districts: A review of existing methods and approaches,” *Renew. Sustain. Energy Rev.*, vol. 135, p. 110206, Jan. 2021, doi: 10.1016/j.rser.2020.110206.

[19] A. Lyden, G. Flett, and P. G. Tuohy, “PyLESA: A Python modelling tool for planning-level Local, integrated, and smart Energy Systems Analysis,” *SoftwareX*, vol. 14, p. 100699, Jun. 2021, doi: 10.1016/j.softx.2021.100699.

[20] “Training,” EnergyPLAN. Accessed: Jul. 29, 2024. [Online]. Available: https://www.energyplan.eu/training/

[21] “MARKAL/TIMES,” EnergyPLAN. Accessed: Jul. 29, 2024. [Online]. Available: https://www.energyplan.eu/othertools/national/markaltimes/

[22] J. Jung and M. Villaran, “Optimal planning and design of hybrid renewable energy systems for microgrids,” *Renew. Sustain. Energy Rev.*, vol. 75, pp. 180–191, Aug. 2017, doi: 10.1016/j.rser.2016.10.061.

[23] H. Lund, J. Z. Thellufsen, P. A. Østergaard, P. Sorknæs, I. R. Skov, and B. V. Mathiesen, “EnergyPLAN – Advanced analysis of smart energy systems,” *Smart Energy*, vol. 1, p. 100007, Feb. 2021, doi: 10.1016/j.segy.2021.100007.

[24] P. A. Østergaard, H. Lund, J. Z. Thellufsen, P. Sorknæs, and B. V. Mathiesen, "Review and validation of EnergyPLAN," *Renew. Sustain. Energy Rev.*, vol. 168, p. 112724, Oct. 2022, doi: 10.1016/j.rser.2022.112724.

[25] P. Sorknæs, H. Lund, and A. N. Andersen, "Future power market and sustainable energy solutions – The treatment of uncertainties in the daily operation of combined heat and power plants," *Appl. Energy*, vol. 144, pp. 129–138, Apr. 2015, doi: 10.1016/j.apenergy.2015.02.041.

[26] P. A. Østergaard and A. N. Andersen, "Optimal heat storage in district energy plants with heat pumps and electrolysers," *Energy*, vol. 275, p. 127423, Jul. 2023, doi: 10.1016/j.energy.2023.127423.

[27] P. A. Østergaard, A. N. Andersen, and P. Sorknæs, "The business-economic energy system modelling tool energyPRO," *Energy*, vol. 257, p. 124792, Oct. 2022, doi: 10.1016/j.energy.2022.124792.

[28] S. Pfenninger, A. Hawkes, and J. Keirstead, "Energy systems modeling for twenty-first century energy challenges," *Renew. Sustain. Energy Rev.*, vol. 33, pp. 74–86, May 2014, doi: 10.1016/j.rser.2014.02.003.

[29] O. Balyk *et al.*, "TIMES-DK: Technology-rich multi-sectoral optimisation model of the Danish energy system," *Energy Strategy Rev.*, vol. 23, pp. 13–22, Jan. 2019, doi: 10.1016/j.esr.2018.11.003.

[30] S. L. Luxembourg, S. S. Salim, K. Smekens, F. D. Longa, and B. van der Zwaan, "TIMES-Europe: An Integrated Energy System Model for Analyzing Europe's Energy and Climate Challenges," *Environ. Model. Assess.*, Jul. 2024, doi: 10.1007/s10666-024-09976-8.

[31] A. Lyden and P. G. Tuohy, "Planning level sizing of heat pumps and hot water tanks incorporating model predictive control and future electricity tariffs," *Energy*, vol. 238, p. 121731, Jan. 2022, doi: 10.1016/j.energy.2021.121731.

[32] O. Dumont, C. Carmo, R. Dickes, E. Georges, and V. Lemort, "Hot water tanks : How to select the optimal modelling approach?," in *Conference CLIMA 2016*, Aalborg, 2016.

[33] Y. Abbassi, E. Baniasadi, and H. Ahmadikia, "Transient energy storage in phase change materials, development and simulation of a new TRNSYS component," *J. Build. Eng.*, vol. 50, p. 104188, Jun. 2022, doi: 10.1016/j.jobe.2022.104188.

[34] A. Wills, C. A. Cruickshank, and I. Beausoleil-Morrison, "Application of the ESP-r/TRNSYS Co-Simulator to Study Solar Heating with a Single-House Scale Seasonal

Storage," *Energy Procedia*, vol. 30, pp. 715–722, Jan. 2012, doi: 10.1016/j.egypro.2012.11.081.

[35] "Welcome | TRNSYS : Transient System Simulation Tool." Accessed: Jul. 30, 2024. [Online]. Available: https://www.trnsys.com/

[36] R. Dickes, A. Desideri, V. Lemort, and S. Quoilin, "Model reduction for simulating the dynamic behavior of parabolic troughs and a thermocline energy storage in a micro-solar power unit," presented at the 28th ECOS conference, Jul. 2015. Accessed: Jul. 29, 2024. [Online]. Available: https://orbi.uliege.be/handle/2268/182681

[37] J. A. Duffie (Deceased), W. A. Beckman, and N. Blair, *Solar Engineering of Thermal Processes, Photovoltaics and Wind*, 1st ed. Wiley, 2020. doi: 10.1002/9781119540328.

[38] R. Franke, "Object-oriented modeling of solar heating systems," *Sol. Energy*, vol. 60, no. 3, pp. 171–180, Mar. 1997, doi: 10.1016/S0038-092X(96)00156-9.

[39] P. Tuohy *et al.*, "Orchestration of Renewable Generation in Low Energy Buildings and Districts Using Energy Storage and Load Shaping," *Energy Procedia*, vol. 78, pp. 2172–2177, Nov. 2015, doi: 10.1016/j.egypro.2015.11.311.

[40] G. Howorth and I. Kockar, "VPP implementations: different types of services developed, experiences and platformsVPP implementations: Grid Services Market 2024," presented at the Grid Services Market 2024, Lucerne KKL Conf Centre, Lucerne, Switzerland, Jul. 2024. Accessed: Aug. 11, 2024. [Online]. Available: https://www.gridservicemarket.com/fileadmin/GSM/2024/Abstr-Paper/GSM-2024_Paper_G0507_10363_VPP%20GH%20IK%20v5.pdf

[41] C. Copeland, G. MacKerron, and T. J. Foxon, "Futures for Findhorn: Exploring challenges for achieving net zero in an ecological intentional community," *Futures*, vol. 149, p. 103155, May 2023, doi: 10.1016/j.futures.2023.103155.

[42] E. H. Owens, "ORIGIN Final Report," 3, Oct. 2015. Accessed: Aug. 11, 2024. [Online]. Available: https://bed.ectp.org/fileadmin/user_upload/documents/BED/ORIGIN/ORIGIN_Final_Report.pdf

[43] "Agile pricing explained," Octopus Energy. Accessed: Aug. 05, 2024. [Online]. Available: https://octopus.energy/blog/agile-pricing-explained/

[44] "Smart Integrated Energy System." Accessed: Aug. 11, 2024. [Online]. Available: https://sies-project.com/

[45] P. Atkinson, A. H. Viklund, R. Doudna, M. Lindner, and S. Stedman, "Park Ecovillage Trust Annual Report FY2022/3." [Online]. Available:

https://parkecovillagetrust.co.uk/wp-content/uploads/2023/06/230530-PET-AnnualReportfy22_3-v4.pdf

[46] "Smart Integrated Energy System - Use Case 6: Findhorn Solar PV & Heat Pump." Accessed: Aug. 11, 2024. [Online]. Available: https://sies-project.com/usecase6.html

[47] C. S. E. Bale, L. Varga, and T. J. Foxon, "Energy and complexity: New ways forward," *Appl. Energy*, vol. 138, pp. 150–159, Jan. 2015, doi: 10.1016/j.apenergy.2014.10.057.

[48] S. A. Adegoke and Y. Sun, "Power system optimization approach to mitigate voltage instability issues: A review," *Cogent Eng.*, vol. 10, no. 1, p. 2153416, Dec. 2023, doi: 10.1080/23311916.2022.2153416.

[49] F. Yu, Q. Guo, J. Wu, Z. Qiao, and H. Sun, "Early warning and proactive control strategies for power blackouts caused by gas network malfunctions," *Nat. Commun.*, vol. 15, no. 1, p. 4714, Jun. 2024, doi: 10.1038/s41467-024-48964-0.

[50] F. R. Badal, P. Das, S. K. Sarker, and S. K. Das, "A survey on control issues in renewable energy integration and microgrid," *Prot. Control Mod. Power Syst.*, vol. 4, no. 1, p. 8, Apr. 2019, doi: 10.1186/s41601-019-0122-8.

[51] D. Wald *et al.*, "Shifting demand: Reduction in necessary storage capacity through tracking of renewable energy generation," *Adv. Appl. Energy*, vol. 10, p. 100131, Jun. 2023, doi: 10.1016/j.adapen.2023.100131.

[52] M. S. Bakare, A. Abdulkarim, M. Zeeshan, and A. N. Shuaibu, "A comprehensive overview on demand side energy management towards smart grids: challenges, solutions, and future direction," *Energy Inform.*, vol. 6, no. 1, p. 4, Mar. 2023, doi: 10.1186/s42162-023-00262-7.

[53] T. Sweetnam, M. Fell, E. Oikonomou, and T. Oreszczyn, "Domestic demand-side response with heat pumps: controls and tariffs," *Build. Res. Inf.*, vol. 47, no. 4, pp. 344–361, May 2019, doi: 10.1080/09613218.2018.1442775.

[54] BMSAdmin, "Building Controls: Optimizing Energy Usage and Comfort in Buildings - BMS Controls and Energy." Accessed: Aug. 12, 2024. [Online]. Available: https://bmscontrols.co.uk/blog/building-controls-optimizing-energy-usage-and-comfort-in-buildings/, https://bmscontrols.co.uk/blog/building-controls-optimizing-energy-usage-and-comfort-in-buildings/

[55] J. Hossain *et al.*, "A Review on Optimal Energy Management in Commercial Buildings," *Energies*, vol. 16, no. 4, Art. no. 4, Jan. 2023, doi: 10.3390/en16041609.

[56] S. R. Jones, J. Beardmore, M. Gillott, R. Boukhanouf, and G. Walker, "A Control Methodology for Building Energy Management Systems (BEMS) in Heat Networks with

Distributed Generation," *Energy Procedia*, vol. 153, pp. 295–302, Oct. 2018, doi: 10.1016/j.egypro.2018.10.011.

[57] C. Chellaswamy, R. Ganesh Babu, and A. Vanathi, "A framework for building energy management system with residence mounted photovoltaic," *Build. Simul.*, vol. 14, no. 4, pp. 1031–1046, Aug. 2021, doi: 10.1007/s12273-020-0735-x.

[58] Y. Gao, Y. Matsunami, S. Miyata, and Y. Akashi, "Model predictive control of a building renewable energy system based on a long short-term hybrid model," *Sustain. Cities Soc.*, vol. 89, p. 104317, Feb. 2023, doi: 10.1016/j.scs.2022.104317.

[59] C. Srithapon and D. Månsson, "Predictive control and coordination for energy community flexibility with electric vehicles, heat pumps and thermal energy storage," *Appl. Energy*, vol. 347, p. 121500, Oct. 2023, doi: 10.1016/j.apenergy.2023.121500.

[60] J. Abushnaf, A. Rassau, and W. Górnisiewicz, "Impact of dynamic energy pricing schemes on a novel multi-user home energy management system," *Electr. Power Syst. Res.*, vol. 125, pp. 124–132, Aug. 2015, doi: 10.1016/j.epsr.2015.04.003.

[61] S. Bechtel, S. Rafii-Tabrizi, F. Scholzen, J.-R. Hadji-Minaglou, and S. Maas, "Influence of thermal energy storage and heat pump parametrization for demand-side-management in a nearly-zero-energy-building using model predictive control," *Energy Build.*, vol. 226, p. 110364, Nov. 2020, doi: 10.1016/j.enbuild.2020.110364.

[62] A. Behzadi and S. Sadrizadeh, "A rule-based energy management strategy for a low-temperature solar/wind-driven heating system optimized by the machine learning-assisted grey wolf approach," *Energy Convers. Manag.*, vol. 277, p. 116590, Feb. 2023, doi: 10.1016/j.enconman.2022.116590.

[63] M. Kuosa *et al.*, "Optimisation of district heating production by utilising the storage capacity of a district heating network on the basis of weather forecasts," *Results Eng.*, vol. 13, p. 100318, Mar. 2022, doi: 10.1016/j.rineng.2021.100318.

[64] M. A. Hassan, S. Serra, S. Sochard, H. Viot, F. Marias, and J.-M. Reneaume, "Optimal scheduling of energy storage in district heating networks using nonlinear programming," *Energy Convers. Manag.*, vol. 295, p. 117652, Nov. 2023, doi: 10.1016/j.enconman.2023.117652.

[65] T. Desguers, A. Lyden, and D. Friedrich, "Integration of curtailed wind into flexible electrified heating networks with demand-side response and thermal storage: Practicalities and need for market mechanisms," *Energy Convers. Manag.*, vol. 304, p. 118203, Mar. 2024, doi: 10.1016/j.enconman.2024.118203.

[66] J. E. T. Bistline, “The importance of temporal resolution in modeling deep decarbonization of the electric power sector,” *Environ. Res. Lett.*, vol. 16, no. 8, p. 084005, Jul. 2021, doi: 10.1088/1748-9326/ac10df.

[67] M. Groissböck, “Are open source energy system optimization tools mature enough for serious use?,” *Renew. Sustain. Energy Rev.*, vol. 102, pp. 234–248, Mar. 2019, doi: 10.1016/j.rser.2018.11.020.

[68] F. Neumann, “Data Science for Energy System Modelling.” Accessed: Jul. 29, 2024. [Online]. Available: https://fneum.github.io/data-science-for-esm/intro.html

[69] A. Lyden, “Modelling and design of local energy systems incorporating heat pumps, thermal storage, future tariffs, and model predictive control,” University of Strathclyde, 2020. Accessed: Jul. 29, 2024. [Online]. Available: https://stax.strath.ac.uk/concern/theses/q811kk106

[70] “odeint — SciPy v1.14.0 Manual.” Accessed: Jul. 29, 2024. [Online]. Available: https://docs.scipy.org/doc/scipy/reference/generated/scipy.integrate.odeint.html

[71] A. M. Khan and M. Osińska, “Comparing forecasting accuracy of selected grey and time series models based on energy consumption in Brazil and India,” *Expert Syst. Appl.*, vol. 212, p. 118840, Feb. 2023, doi: 10.1016/j.eswa.2022.118840.

[72] D. R. Landsberg *et al.*, *ASHRAE Guideline 14 - Measurement of Energy, Demand, and Water Savings*, Dec. 18, 2014. Accessed: Aug. 01, 2024. [Online]. Available: https://upgreengrade.ir/admin_panel/assets/images/books/ASHRAE%20Guideline%2014-2014.pdf

[73] “Kinloss (Moray) weather - Met Office.” Accessed: Aug. 04, 2024. [Online]. Available: https://www.metoffice.gov.uk/weather/forecast/gfjryyz20#?date=2024-08-04

[74] Thermostatic Mixing Valve Manufacturers Association, “Recommended Code of Practice for Safe Water Temperatures.” Mar. 2000. Accessed: Aug. 04, 2024. [Online]. Available: https://www.beama.org.uk/asset/022A6360-7B36-4F5B-A192238D9C4F896E/

[75] I. Staffell and R. Green, “How does wind farm performance decline with age?,” *Renew. Energy*, vol. 66, pp. 775–786, Jun. 2014, doi: 10.1016/j.renene.2013.10.041.

[76] “Variability of annual generation of wind, solar PV and hydropower in selected countries – Charts – Data & Statistics,” IEA. Accessed: Aug. 11, 2024. [Online]. Available: https://www.iea.org/data-and-statistics/charts/variability-of-annual-generation-of-wind-solar-pv-and-hydropower-in-selected-countries

[77] T. Kara and A. D. Şahin, “Implications of Climate Change on Wind Energy Potential,” *Sustainability*, vol. 15, no. 20, Art. no. 20, Jan. 2023, doi: 10.3390/su152014822.

[78] A. R. Silva, D. A. C. Narciso, L. C. Gomes, F. G. Martins, L. F. Melo, and A. Pereira, “Proof-of-concept approach to assess the impact of thermal disinfection on biofilm structure in hot water networks,” *J. Water Process Eng.*, vol. 53, p. 103595, Jul. 2023, doi: 10.1016/j.jwpe.2023.103595.

[79] J. Stute and M. Klobasa, “How do dynamic electricity tariffs and different grid charge designs interact? - Implications for residential consumers and grid reinforcement requirements,” *Energy Policy*, vol. 189, p. 114062, Jun. 2024, doi: 10.1016/j.enpol.2024.114062.

[80] P. Stoffel, M. Berktold, and D. Müller, “Real-life data-driven model predictive control for building energy systems comparing different machine learning models,” *Energy Build.*, vol. 305, p. 113895, Feb. 2024, doi: 10.1016/j.enbuild.2024.113895.

[81] J. Drgoňa *et al.*, “All you need to know about model predictive control for buildings,” *Annu. Rev. Control*, vol. 50, pp. 190–232, Jan. 2020, doi: 10.1016/j.arcontrol.2020.09.001.

[82] S. Zhang, P. Ocłoń, J. J. Klemeš, P. Michorczyk, K. Pielichowska, and K. Pielichowski, “Renewable energy systems for building heating, cooling and electricity production with thermal energy storage,” *Renew. Sustain. Energy Rev.*, vol. 165, p. 112560, Sep. 2022, doi: 10.1016/j.rser.2022.112560.

9.0 Appendix 1 – DHW Heat Loss Parameter Calibration

Calibration of heat loss parameters was conducted using monitored data between timesteps 14592 and 14605. No charging or discharging events occurred during this period. The final calibrated heat loss parameters are [2.5, 2, 2.5, 8, 30]. Model node temperatures using these parameters are compared against monitored temperatures in Figures 15, 16, 17, 18, and 19.

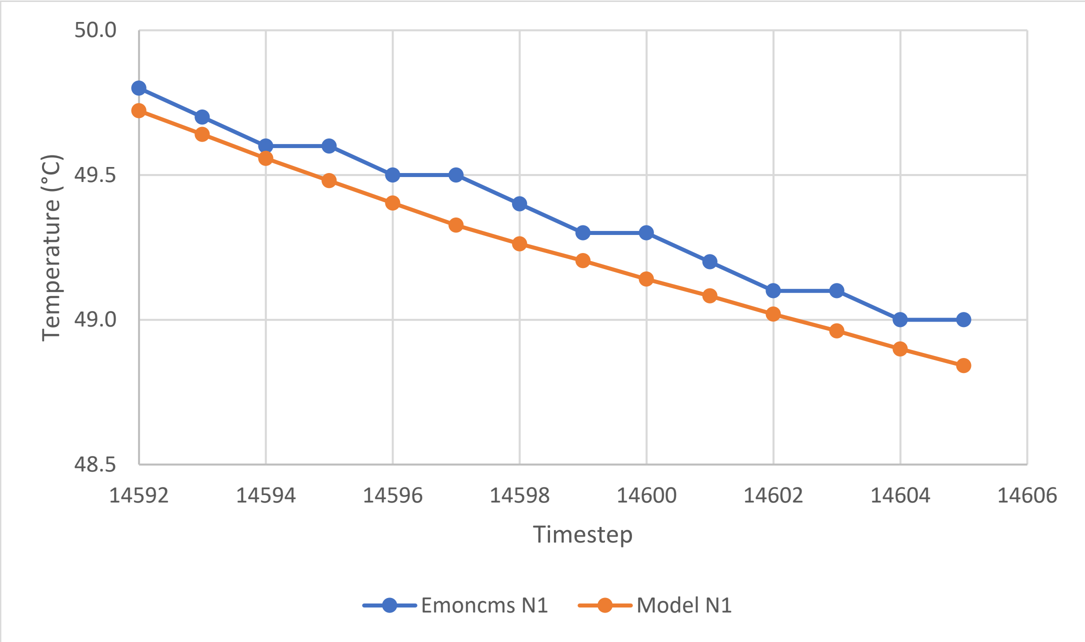

Figure 15. Monitored and modelled top node temperatures using calibrated heat loss parameters.

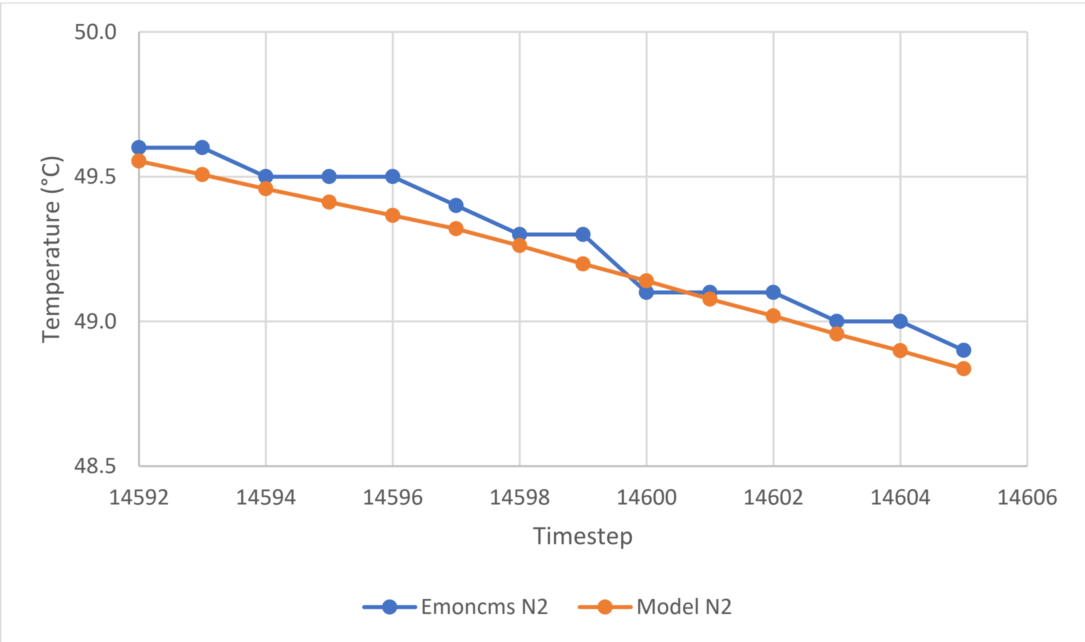

Figure 16. Monitored and modelled second node temperatures using calibrated heat loss parameters.

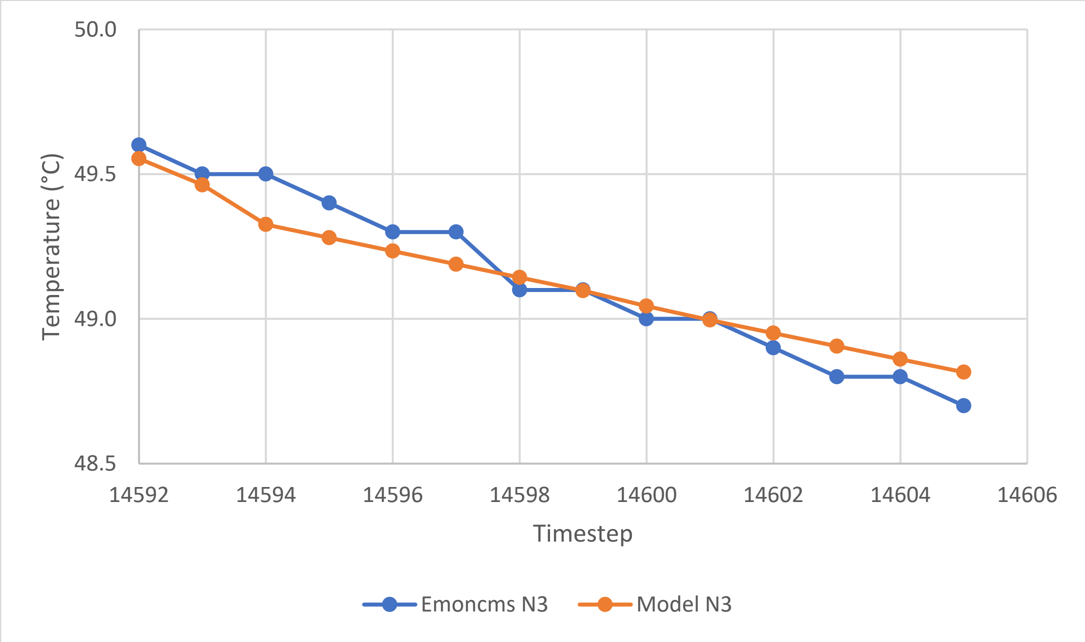

Figure 17. Monitored and modelled third node temperatures using calibrated heat loss parameters.

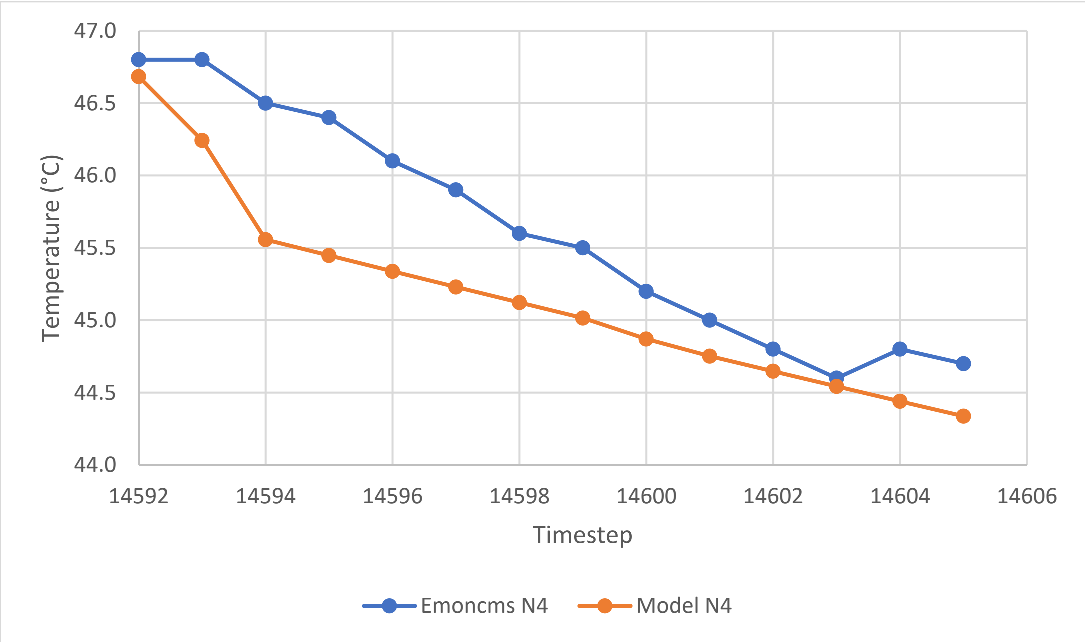

Figure 18. Monitored and modelled fourth node temperatures using calibrated heat loss parameters.

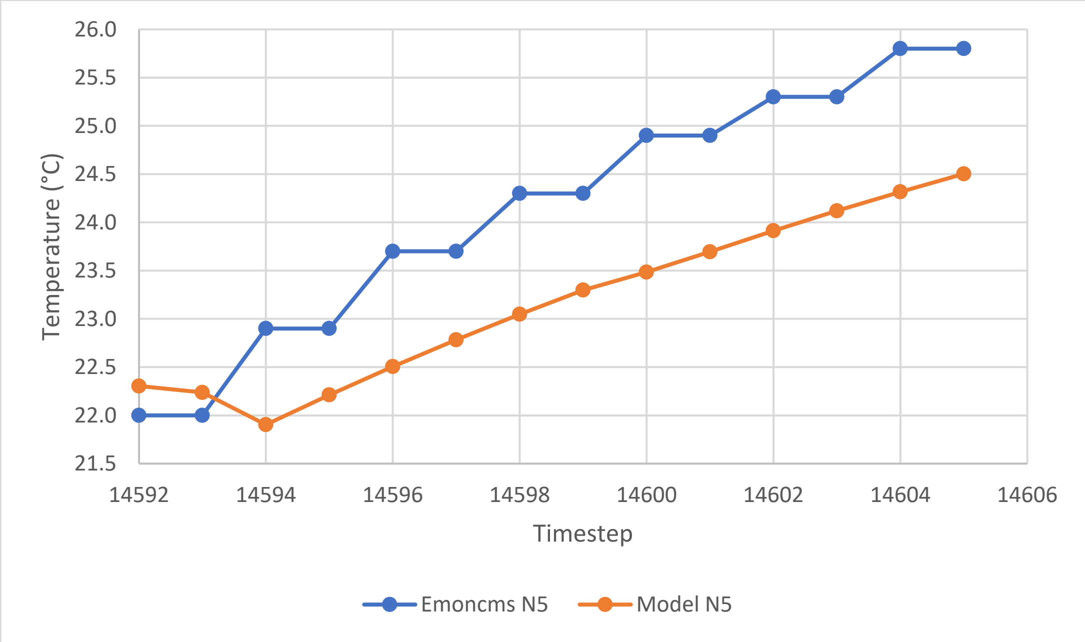

Figure 19. Monitored and modelled fourth node temperatures using calibrated heat loss parameters.

10.0 Appendix 2 – Additional Simulation Results

This Appendix contains additional simulation results not presented in the main body of the thesis. These results include annual totals for electricity used to charge the SH and DHW tanks; thermal charge to the SH and DHW tanks; electricity usage from PV, wind, and grid imports; total carbon emissions; and thermal discharge from SH and DHW.

Table 9. Total electrical charge, thermal charge, and thermal discharge across simulated control and tariff scenarios.

Control	*Tariff*	*Electrical Charge (kWh_e)*	*Thermal Charge (kWh_{th})*	*Thermal Discharge (kWh_{th})*
Demand-Led RBC	*Standard*	7172	17756	14822
	Day-night	7172	17756	14822
	DWT 1	7172	17756	14822
	DWT 2	7172	17756	14822
	DWT 3	7172	17756	14822
Opportunistic PV RBC	*Standard*	7252	17864	14822
	Day-night	7252	17864	14822
	DWT 1	7252	17864	14822
	DWT 2	7253	17864	14822
	DWT 3	7253	17864	14822
Advanced RBC (SH seasonally disabled)	*Standard*	7188	17532	14822
	Day-night	7188	17532	14822
	DWT 1	7188	17532	14822
	DWT 2	7189	17532	14822
	DWT 3	7189	17532	14822
Advanced RBC (SH not seasonally disabled)	*Standard*	6996	17062	14822
	Day-night	6996	17062	14822
	DWT 1	6996	17062	14822
	DWT 2	6996	17062	14822
	DWT 3	6996	17062	14822

Table 10. Total DHW electrical charge, thermal charge, and thermal discharge across simulated control and tariff scenarios.

Control	*Tariff*	*DHW Electrical Charge (kWh_e)*	*DHW Thermal Charge (kWh_{th})*	*DHW Thermal Discharge (kWh_{th})*
Demand-Led RBC	*Standard*	2193	6034	4754
	Day-night	2193	6034	4754
	DWT 1	2193	6034	4754
	DWT 2	2193	6034	4754
	DWT 3	2193	6034	4754
Opportunistic PV RBC	*Standard*	2220	6055	4754
	Day-night	2220	6055	4754
	DWT 1	2220	6055	4754
	DWT 2	2220	6055	4754
	DWT 3	2220	6055	4754
Advanced RBC (SH seasonally disabled)	*Standard*	2200	5915	4754
	Day-night	2200	5915	4754
	DWT 1	2200	5915	4754
	DWT 2	2199	5915	4754
	DWT 3	2199	5915	4754
Advanced RBC (SH not seasonally disabled)	*Standard*	2199	5915	4754
	Day-night	2199	5915	4754
	DWT 1	2199	5915	4754
	DWT 2	2199	5915	4754
	DWT 3	2199	5915	4754

Table 11. Total SH electrical charge, thermal charge, and thermal discharge across simulated control and tariff scenarios.

Control	Tariff	SH Electrical Charge (kWh_e)	SH Thermal Charge (kWh_{th})	SH Thermal Discharge (kWh_{th})
Demand-Led RBC	Standard	4979	11722	10068
	Day-night	4979	11722	10068
	DWT 1	4979	11722	10068
	DWT 2	4980	11722	10068
	DWT 3	4980	11722	10068
Opportunistic PV RBC	Standard	5032	11809	10068
	Day-night	5032	11809	10068
	DWT 1	5032	11809	10068
	DWT 2	5032	11809	10068
	DWT 3	5032	11809	10068
Advanced RBC (SH seasonally disabled)	Standard	4988	11617	10068
	Day-night	4988	11617	10068
	DWT 1	4988	11617	10068
	DWT 2	4988	11617	10068
	DWT 3	4988	11617	10068
Advanced RBC (SH not seasonally disabled)	Standard	4797	11147	10068
	Day-night	4797	11147	10068
	DWT 1	4797	11147	10068
	DWT 2	4797	11147	10068
	DWT 3	4797	11147	10068

Table 12. Total PV, wind, and grid electricity used for tank charging across simulated control and tariff scenarios.

Control	Tariff	PV Used to Charge (kWh_e)	Wind Used to Charge (kWh_e)	Grid Used to Charge (kWh_e)
Demand-Led RBC	Standard	829	1827	4516
	Day-night	829	1827	4516
	DWT 1	829	1827	4516
	DWT 2	829	1827	4516
	DWT 3	829	1827	4516
Opportunistic PV RBC	Standard	1316	1681	4256
	Day-night	1316	1681	4256
	DWT 1	1316	1681	4256
	DWT 2	1316	1681	4256
	DWT 3	1316	1681	4256
Advanced RBC (SH seasonally disabled)	Standard	1315	2461	3411
	Day-night	1315	2461	3411
	DWT 1	1315	2461	3411
	DWT 2	1315	2461	3412
	DWT 3	1315	2461	3412
Advanced RBC (SH not seasonally disabled)	Standard	1149	2433	3413
	Day-night	1149	2433	3413
	DWT 1	1149	2433	3413
	DWT 2	1149	2433	3413
	DWT 3	1149	2433	3413